Efficient methods for multiple types of precise gene-editing in Chlamydomonas

Chen, Hui; Yang, Qing-Lin; Xu, Jia-Xi; Deng, Xuan; Zhang, Yun-Jie; Liu, Ting; Rots, Marianne G; Xu, Guo-Liang; Huang, Kai-Yao

Published in:
Plant Journal

DOI:
10.1111/tpj.16265

the plant journal

SEB SOCIETY FOR EXPERIMENTAL BIOLOGY

The Plant Journal (2023) **115,** 846–865 doi: 10.1111/tpj.16265

TECHNICAL ADVANCE

Efficient methods for multiple types of precise gene-editing in *Chlamydomonas*

Hui Chen[1,*,†], Qing-Lin Yang[1,†,‡], Jia-Xi Xu[1,2], Xuan Deng[3], Yun-Jie Zhang[3], Ting Liu[1,4], Marianne G. Rots[5], Guo-Liang Xu[1,4,6] and Kai-Yao Huang[3,*]

[1]*State Key Laboratory of Molecular Biology, Shanghai Institute of Biochemistry and Cell Biology, Center for Excellence in Molecular Cell Science, Chinese Academy of Sciences, Shanghai 200031, China,*

[2]*University of Chinese Academy of Sciences, Beijing 100049, China,*

[3]*Key Laboratory of Algal Biology, Institute of Hydrobiology, Chinese Academy of Sciences, Wuhan 430072, China,*

[4]*School of Life Science and Technology, ShanghaiTech University, Shanghai 201210, China,*

[5]*Department of Pathology and Medical Biology, University of Groningen, University Medical Center Groningen, 9713 GZ, Groningen, The Netherlands,*

[6]*Shanghai Key Laboratory of Medical Epigenetics, Laboratory of Cancer Epigenetics, Institutes of Biomedical Sciences, Medical College of Fudan University, Chinese Academy of Medical Sciences (RU069), Shanghai, China*

Received 2 February 2023; revised 20 April 2023; accepted 26 April 2023; published online 28 April 2023.
*For correspondence (e-mail chenhui01@sibs.ac.cn and huangky@ihb.ac.cn).
†These authors are contributed equally to this work.
‡Present address: University of Texas Southwestern Medical Center, Dallas, TX, USA

SUMMARY

Precise gene-editing using CRISPR/Cas9 technology remains a long-standing challenge, especially for genes with low expression and no selectable phenotypes in *Chlamydomonas reinhardtii*, a classic model for photosynthesis and cilia research. Here, we developed a multi-type and precise genetic manipulation method in which a DNA break was generated by Cas9 nuclease and the repair was mediated using a homologous DNA template. The efficacy of this method was demonstrated for several types of gene editing, including inactivation of two low-expression genes (*CrTET1* and *CrKU80*), the introduction of a *FLAG-HA* epitope tag into *VIPP1*, *IFT46*, *CrTET1* and *CrKU80* genes, and placing a *YFP* tag into *VIPP1* and *IFT46* for live-cell imaging. We also successfully performed a single amino acid substitution for the *FLA3*, *FLA10* and *FTSY* genes, and documented the attainment of the anticipated phenotypes. Lastly, we demonstrated that precise fragment deletion from the 3′-UTR of *MAA7* and *VIPP1* resulted in a stable knock-down effect. Overall, our study has established efficient methods for multiple types of precise gene editing in *Chlamydomonas*, enabling substitution, insertion and deletion at the base resolution, thus improving the potential of this alga in both basic research and industrial applications.

Keywords: efficient, multi-type, homology-mediated, precision, gene-editing, *Chlamydomonas*.

INTRODUCTION

Thanks to the simplicity, effectiveness and various design possibilities, CRISPR/Cas9 has become one of the most widely utilized genetic manipulation tools in many model organisms, such as bacteria, yeast, plants and mammals (Jakočiūnas et al., 2015; Jiang et al., 2013; Mali et al., 2013; Ran et al., 2013; Singh et al., 2017, 2018). In stark contrast to the ease in several organisms, gene-editing rates remain low in *Chlamydomonas reinhardtii* (hereafter, *Chlamydomonas*), a unicellular green alga widely used as a model for photosynthesis and cilia research (Merchant et al., 2007). Although earlier work demonstrated the feasibility of gene editing using the CRISPR/Cas9 system in *Chlamydomonas*, the efficiency has remained extremely low (Jiang et al., 2014). More specifically, the continuous expression of Cas9 protein caused apparent toxicity in *Chlamydomonas* cells, resulting in low edited mutant yields (Jiang et al., 2014; Jiang & Weeks, 2017). Recently, several laboratories have succeeded in generating targeted gene mutations with selectable phenotypes by delivering

Cas9-gRNA ribonucleoproteins (RNPs) directly into the cells of *Chlamydomonas* (Akella et al., 2021; Baek et al., 2016; Dhokane et al., 2020; Greiner et al., 2017; Guzmán-Zapata et al., 2019; Jeong et al., 2018; Jiang et al., 2014; Jiang & Weeks, 2017; Shin et al., 2016). Meanwhile, the co-delivery of Cpf1-gRNA RNPs with a single-stranded DNA (ssDNA) repair template resulted in sequence-specific mutations and epitope tagging at an endogenous locus (Ferenczi et al., 2017). These methods facilitated screening the mutants for the genes whose loss-of-function mutation causes visible and known phenotypes. Subsequently, mutants for genes with non-selectable phenotypes were obtained by co-selection either with an exogenous antibiotic-resistant cassette (Findinier et al., 2019; Greiner et al., 2017; Kim et al., 2020; Picariello et al., 2020; Shamoto et al., 2018; Shin et al., 2016) or with mutation of an endogenous gene that produced a dominant selectable phenotype (Akella et al., 2021; Xue et al., 2019). Furthermore, Cas9-gRNA RNP was used for homology-directed integration of antibiotic resistance cassette to inactivate genes (Angstenberger et al., 2020; Picariello et al., 2020) or for insertion of a FLAG-tag to facilitate the detection of gene products (Greiner et al., 2017), or an amino acid substitution of the *ALS* gene to acquire herbicide resistance (Jiang & Weeks, 2017).

These studies pinpointed the importance of the repair templates and the feasibility of introducing the Cas9-gRNA RNP into cells for gene editing. Nevertheless, for genes with low transcription levels, such as *FTSY*, *SRP43* and *CrKU80*, the mutant isolation efficiency was still low, with most mutants carrying unpredicted deletions or insertions (Akella et al., 2021; Greiner et al., 2017) at the target site. In addition, precise genetic manipulation such as knock-in of DNA sequences encoding an epitope tag or a fluorescent tag targeting the N-terminus or C-terminus of the protein, or precise substitution of an amino acid at any desired site of the protein is not easy with current methods and the new approach is valuable.

Currently, because a complete knock-out (null mutant) of essential genes cannot be obtained in *Chlamydomonas*, the functional studies of these genes rest on knock-down mutants generated by artificial MicroRNAs (Hu et al., 2014; Molnár et al., 2009; Rohr et al., 2004; Schmollinger et al., 2010; Zhao et al., 2009). However, epigenetic silencing often inhibits the expression of transgenic DNA (Neupert et al., 2020) and artificial MicroRNA (Hu et al., 2014), resulting in progressisive loss of the knock-down effect on target genes. Recently, a study in mammalian cells showed that deletion in the 3′-UTR of a target gene using CRISPR/Cas9 reduced not only the transcirption of the target gene but also the stability of the mRNA (Zhao, Siegel, et al., 2017). Such a gene knock-down method based on CRISPR/Cas9 has not been reported in *Chlamydomonas*.

Therefore, further efforts are needed to improve the knock-out efficiency for the low-transcription genes and to develop robust approaches for precise gene editing, including the knock-in of an epitope tag or a fluorescent tag, the substitution of amino acid at a specific site, and deletion of a DNA fragment in a given gene in *Chlamydomonas*. We therefore considered potential DNA repair pathways relevant to gene editing in *Chlamydomonas*. Non-homologous end-joining (NHEJ) often introduces unpredicted indels, whereas homology-directed repair (HDR) plays a crucial role in repairing DNA double-strand breaks (DSBs) in most organisms (Thompson & Schild, 2001; Zhao, Steinfeld, et al., 2017). Microhomology-mediated end-joining (MMEJ) requires micro-homologous sequences (5–25 bp) for DSB repair, resulting in error-prone end-joining or knock-in with intact donor DNA (Bae et al., 2014; McVey & Lee, 2008; Sakuma et al., 2016).

The most common strategies for precise gene editing rely on homologous recombination (HR; Hockemeyer et al., 2011; Yang et al., 2013). The canonical HR usually requires a repair template containing left and right homology DNA arms of 500–2000 bp. But the efficiency of HR varies across species and is extremely low in *Chlamydomonas* (Sodeinde & Kindle, 1993). The use of long arms for HR is also complicated by the increased possibility of donor DNA digestion by endogenous nucleases and random insertion of the donor DNA into the *Chlamydomonas* genome (Akella et al., 2021; Greiner et al., 2017; Zhang et al., 2014). MMEJ-based editing using 25-bp micro-homologous arms combined with the CRISPR/Cas9 system has enabled precise knock-in at target sites in worms, frogs, human cells, zebrafish, yeast and *Chlamydomonas* (Hayashi & Tanaks, 2019; Hisano et al., 2015; Nakade et al., 2014; Picariello et al., 2020). More recently, NHEJ, HR and MMEJ were shown to contribute to the repair of CRISPR/Cas9-induced DSBs in *Chlamydomonas*, with MMEJ playing a predominant role (Akella et al., 2021; Ferenczi et al., 2021; Sizova et al., 2021). This knowledge had not yet been applied to engineering *Chlamydomonas* strains, but it did suggest that providing a donor with microhomology may facilitate precise gene editing via DNA integration in *Chlamydomonas*.

In this study, we developed efficient methods for multiple types of precise gene editing in *Chlamydomonas* based on homology-mediated recombination. This system comprised rational donor design, optimization of targeting strategies, generation of drug-resistant co-transformant libraries, polymerase chain reaction (PCR) screening, and functional analysis of resultant transformants. The efficacy of this system for precise genetic manipulations such as knock-in of an epitope tag or a fluorescent tag, amino acid substitution, and DNA fragment deletion was demonstrated.

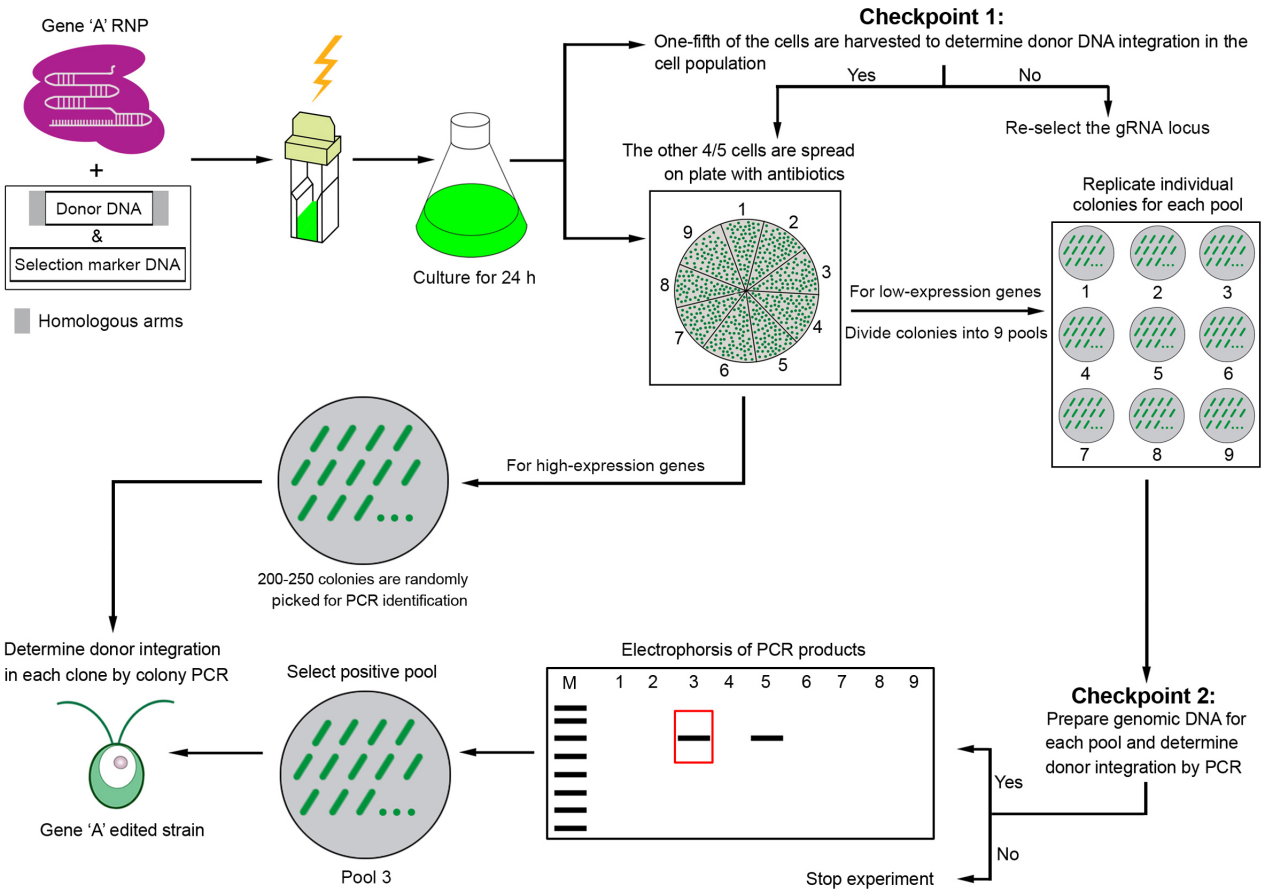

Figure 1. Strategy of homology-directed donor DNA integration for the isolation of precisely edited mutants.
Cells are transformed with a gene-specific gRNA/Cas9 ribonucleoprotein (RNP) together with a dsDNA donor and a selectable marker cassette. Double-stranded (ds)DNA donors contain at both ends a homologous arm corresponding to the flanking sequence of the Cas9 cut site in the target gene. Two checkpoints are set in the screening protocol. As checkpoint 1, the occurrence of integration is first confirmed at the population level, and then a choice of further screens is decided according to the expression level of the target gene. Checkpoint 1 is used to screen the efficient gRNA target sites and to decide whether there is a need to continue the screening. For high-expression genes, 200–250 resistant colonies are picked for PCR screen. For low-expression genes, the colonies are divided into nine pools and the pool containing a mutant is determined using PCR (checkpoint 2). Checkpoint 2 is used to identify the pools that contain the expected clones among the nine resistant clone pools quickly. As an example, the red rectangle box indicates that the genomic DNA from the #3 pool contains the candidate clones with donor DNA integrated at the gRNA site. Individual colonies in the PCR-positive pool are then screened to isolate the mutants with the desired edit.

RESULTS

Developing a homology-mediated integration-dependent screening pipeline

The mutants for the gene with non-selectable phenotypes were obtained by co-knocking out an endogenous gene such as *MAA7* or *PPX1* in *Chlamydomonas* (Akella et al., 2021; Xue et al., 2019). The isolation efficiency for high-expression target genes *VTC2* and *FTSY* was higher compared with that of low-expression genes *CrTET1* and *WDTC1* (Akella et al., 2021; Xue et al., 2019; Table S2). We also successfully isolated the mutant for another three genes (*FKB12*, *FTSY*, *IFT46*) using the same *MAA7*-based co-selection strategy (Figure S1). However, we failed to identify mutants for the low-expression gene *CrKU80* from more than 96 5-FI-resistant colonies. To isolate the mutants for the low-expression genes such as *CrKU80*, we developed a pipeline based on homology-mediated donor DNA integration (Figure 1). Cells were transformed with a gene-specific gRNA/Cas9 RNP combined with a short or long double-strand (ds)DNA donor containing homologous arms at either end. These arms were homologous to the flanking sequence of the respective Cas9 cut site, facilitating microhomology-mediated donor DNA integration at the DSB (Picariello et al., 2020).

To ensure success, a targeted integration-dependent screening protocol harboring two checkpoints was developed (Figure 1). The integration event was first confirmed at the whole cell population level. For each target gene, one electroporation cell (or mixed two electroporation cells) were recovered for 24 h. Subsequently, 1/5 of the cells were harvested to isolate genomic DNA, which was used to

determine whether the donor DNA integration occurred at the Cas9 cut site using nested PCR and DNA sequencing. We referred to this step as checkpoint 1 (Figure 1). Meanwhile, the remaining 4/5 cells were plated on a Tris/acetate/phosphate (TAP)-agar plate containing antibiotics to obtain single resistant colony following the general transformation procedure. The mutant screening protocol was optimized according to the expression level of the target gene (Figure 1). For the genes with low-expression levels (e.g. FPKM < 5), the antibiotic-resistant clones on the original plates (about 1000 clones) were divided into nine pools, the colonies in each pool were replicated into a new plate using toothpick or QPix 400 Series Microbial Colony Picker (Molecular Devices, LLC, San Jose, CA, USA), and the remaining cells in each pool were mixed to determine which pools contained the mutant using nested PCR. This step was designated as checkpoint 2. Only when the pool was confirmed to contain the desired mutant, individual colonies in this pool were screened to isolate the mutant (Figure 1).

Given that only one *CrTET1* mutant was obtained from 986 5-FI-resistant colonies in the previous study (Xue et al., 2019), and no *CrKU80* mutants were obtained from 200 5-FI-resistant colonies (Figure S1), *CrTET1* and *CrKU80* were selected to determine the mutant isolation efficiency using the above screening pipeline (Figure S2a). CC-5325 cells were either transformed with *CrTET1* Cas9/RNPs together with micro-homologous donor DNA containing hygromycin resistance (Hm^R) gene expression cassette, or *CrKU80* Cas9/RNPs together with donor DNA containing paromomycin resistance (Pm^R) gene expression cassette. At checkpoint 1, the obtained predicted nested PCR products confirmed that donor DNA was integrated into the Cas9 cut site in *CrTET1* and *CrKU80* at the cell population level (Figure S2b). Then, all the Hm^R or Pm^R colonies were divided into nine pools (Figure S2c,d).

At checkpoint 2, nested PCR amplification results showed that Hm^R pools #1, #3, #4, #7 and #8 contained candidate *CrTET1* mutants (Figure S2c). In the #1 Hm^R pool, the PCR results showed that integration of the Hm^R cassette occurred in clones #5, #21, #23, #24, #33 and #54 (Figure S2e). To verify whether the integration of complete donor DNA occurred at the Cas9 cut site, we amplified a ~3.0-kb PCR product in four *CrTET1* mutants (#21, #23, #24 and #54), whereas only 1.3 kb was obtained in the wild-type (WT) strain (Figure S2g,h). Interestingly, in #5 and #33 *CrTET1* mutants, a band of approximately 5 kb was amplified. Sequencing of these PCR products showed that two donor DNA fragments were serially integrated into the Cas9 cut site with a 17-bp linker DNA fragment originating from *Cre16.g675350* on chromosome 16 (Figure S2g; Table S4). Using the same screening method, we identified nine colonies harboring an integrating DNA donor at the *CrTET1*-gRNA1 target site from the #3, #4, #7 and #8 Hm^R pools. Fifteen *CrTET1* mutants were isolated from 540 Hm^R colonies with an editing efficiency of 2.8% (15/540; Figure S2j).

Nested PCR results showed that pools #3, #4 and #7 contained putative *CrKU80* mutants (Figure S2d). Five colonies harboring an integrated DNA donor at the *CrKU80*-gRNA1 target site were identified from the #3 Pm^R pool (Figure S2f–h). Spot growth experiments containing low dose of the DNA-damaging agent zeocin showed *CrKU80* mutant cells were more sensitive to zeocin than WT cells (Figure S2i), consistent with previous reports (Ferenczi et al., 2021; Rohr et al., 2004; Sizova et al., 2021). These data indicated that the null mutation of *CrKU80* was obtained. In addition, two clones with an integrated DNA donor at the *CrKU80*-gRNA target site were identified from the #4 Pm^R pool. In total, seven *CrKU80* mutants were isolated from 540 Pm^R colonies with an editing efficiency of 1.3% (7/540; Figure S2j). The mutant isolation efficiency was substantially improved compared with the co-selection strategy with *MAA7* (Xue et al., 2019).

Microhomology-mediated integration of short donor DNA containing stop codons for target gene inactivation

Short donor DNA is more efficiently integrated into DSBs than long donor DNA (Greiner et al., 2017). Hence, we assessed whether the use of short donor DNA can further improve the integration efficiency. The low-expression gene *CrKU80* was chosen, and the three gRNA target sites were selected (Figure 2a). A 96-bp dsDNA donor including a 56-bp DNA fragment containing a stop codon in each reading frame with 20-bp micro-homologous arms on each side was designed as the DSB repair template (Tables S1 and S3). At the whole cell population level, the integration efficiency of 96-bp dsDNA varied at different gRNA target sites, and the integration efficiency was the highest at *CrKU80*-gRNA2 target site and the lowest at *CrKU80*-gRNA1 target site (Figure 2b).

To compare the gene-editing efficiency with the long donor DNA, we first focused on the *CrKU80*-gRNA1 target site, which was used previously. The PCR products of 20 clones were of different sizes from 200 randomly selected Hm^R colonies compared with the WT cells (Figure 2c). Subsequently, we sequenced the PCR products and confirmed that all 20 clones were edited at the *CrKU80*-gRNA1 locus, among which 16 were imprecisely edited, and four were precisely edited (Figure 2d). The total editing efficiency of the *CrKU80*-gRNA1 target was 10% (20/200), and the precision-editing efficiency was 2% (4/200; Figure 2e). Therefore, for the same *CrKU80*-gRNA1 target locus, the total editing efficiency using the short donor DNA was improved by more than seven times (10%/1.3%) compared with that using the long donor DNA (Figure S2j).

Using the same screening strategy, we isolated 58 edited clones at the *CrKU80*-gRNA2 target locus from randomly selected 200 Hm^R colonies, among which 12 clones

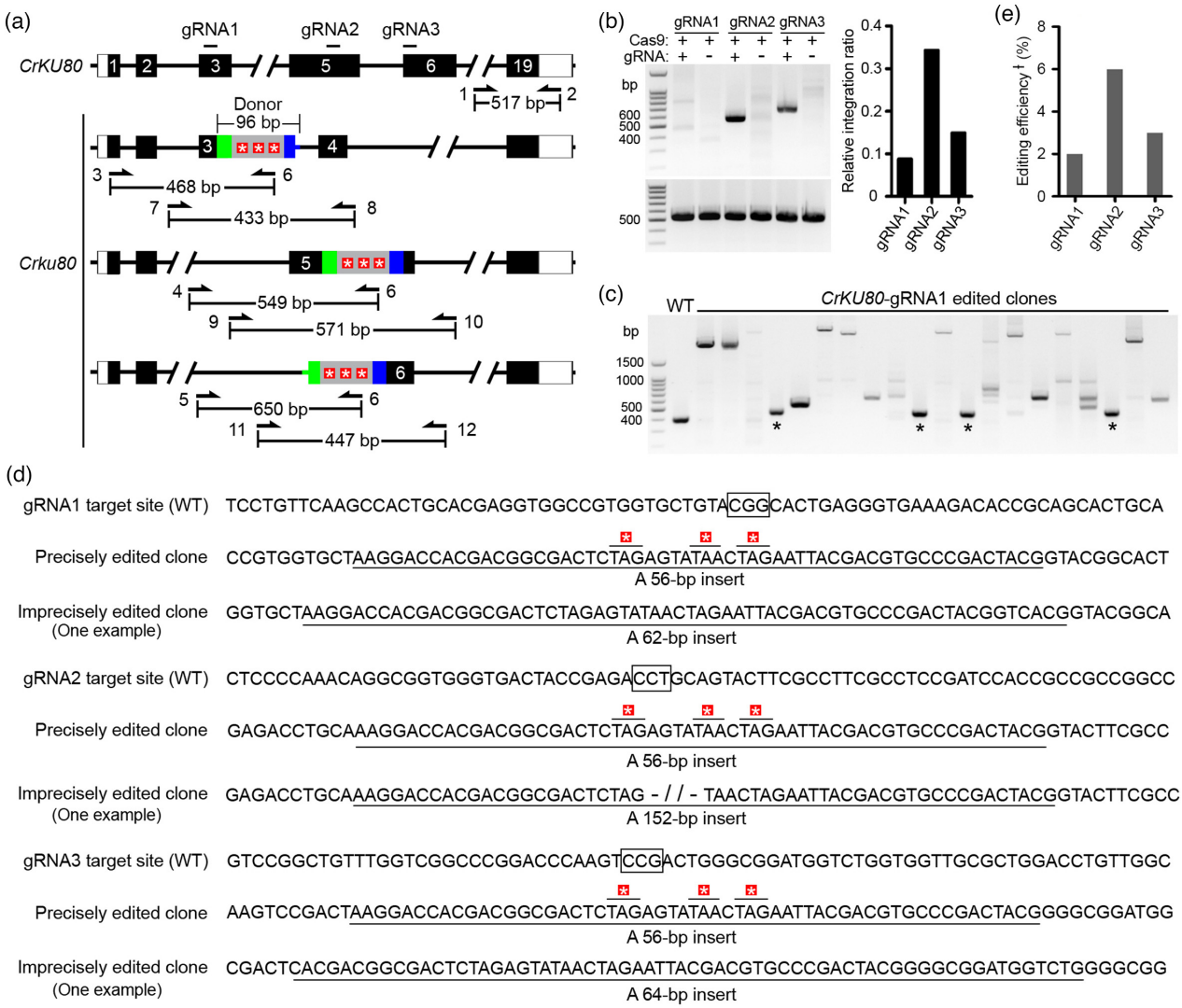

Figure 2. Targeted inactivation of low-expression *CrKU80* by inserting a short sequence containing stop codons into a coding exon.
(a) Schematic of the *CrKU80* gene with three gRNA target sites. The predicted genetic maps with the insertion of a 96-bp donor into the Cas9 cut site are given below. Primer pairs used for polymerase chain reaction (PCR) and the size of expected products are indicated. Green and blue colors highlight the genomic regions used as microhomology arms.
(b) Comparison of the donor integration rates at the three gRNA target sites. Semi-quantitative PCR was performed for the whole cell population of the overnight liquid culture upon electroporation. The lower left gel picture shows the amplified DNA fragment at the 3′-terminal of *CrKU80* (away from the three gRNA target sites) was used to normalize genomic DNA input.
(c) Twenty putative mutants with donor integration at the *CrKU80*-gRNA1 locus were identified from 200 randomly selected hygromycin resistance (Hm^R) colonies. Four potential precision-edited mutants with PCR products of an anticipated size are marked with asterisks.
(d) Confirmation of donor integration by DNA sequencing. The sequences of *CrKU80* in the wild-type (WT), precision-edited and imprecision-edited clones are shown. The insertion at the Cas9 cut site is underlined, and the stop codons are marked with red squares. The rectangular box indicates the PAM nucleotides.
(e) The editing efficiency of the three *CrKU80* loci in 200 randomly selected Hm^R colonies. [‡]In this study, editing efficiency is defined as the number of precisely edited clones over the number of screened resistant clones, excluding undesired imprecisely edited mutants.

were precisely edited with an efficiency of 6% (12/200; Figures 2d,e and S3a). For the *CrKU80*-gRNA3 target locus, DNA sequencing confirmed that 24 clones were edited, and six clones were precisely edited with an efficiency of 3% (6/200; Figures 2d,e and S3b). These results demonstrated that the null mutants of the low-expressed *CrKU80* gene were successfully obtained at multiple target sites using the method of microhomology-mediated integration of donor DNA, and the short donor DNA, including stops codon, distinctly increased the gene-editing efficiency.

To demonstrate that our method can also be applied to different *Chlamydomonas* strains, we selected *FTSY* as a target gene using the CC-1328 strain, as mutation of FTSY resulted in a distinct light-green color compared with the dark-green WT cells (Baek et al., 2016). Ten days after delivering *FTSY* Cas9/RNPs together with a 96-bp dsDNA

containing stop codons (Figure S4a) and Hm^R gene expression cassette into cells (Table S1), the Hm^R colonies were photographed, and some colonies showed distinct light-green colors (Figures S4b and S5a). Twenty-six light-green colonies were replicated to a new plate (Figure S4b). PCR products with different sizes compared with WT cells were obtained in 12 out of the 26 light-green clones (Figure S3g). Sequencing of these products confirmed that a 96-bp DNA donor was precisely integrated at the Cas9 cut site in six clones (Figure S4c). The total editing efficiency at the *FTSY*-gRNA1 target site was 6.2% (26/416), and the precise knock-in efficiency of DNA fragments was 1.4% (6/416; Figure S4d). These data demonstrated that micro-homologous arms could effectively mediate precise knock-in of donor DNA at the target site in multiple strains of *Chlamydomonas*.

Microhomology-mediated knock-in of the *FLAG-HA* epitope tag

Considering the microhomology-mediated integration of donor DNA showed a promising precise-editing efficiency, we tested whether this strategy was suitable for knocking in an epitope tag in the coding sequence. *VIPP1* and *IFT46* were selected as target genes because their functions and subcellular localization have been well studied (Hou et al., 2007; Nordhues et al., 2012). VIPP1 is a chloroplast component and IFT46 is an intraflagellar transporter. We determined a PAM sequence close to the stop codon in the last exon of *VIPP1* or *IFT46* (Figure 3a). The DNA donor used included a 54-bp DNA fragment containing a *FLAG-HA* coding sequence, a stop codon, and 21–22-bp micro-homologous arms at either end (Figure 3a; Tables S1 and S3). Nested PCR confirmed that the donor was integrated at the Cas9 cut site of *VIPP1* and *IFT46* on the cell population level in the host strain CC-5325 (Figure 3b).

For the *VIPP1*-gRNA target locus, 19 putative edited clones from 250 randomly selected Hm^R colonies were identified based on their PCR product size larger than 369 bp. Among them, PCR products of nine clones had a predicted size of ~420 bp (Figure S3c). DNA sequencing confirmed that the *FLAG-HA* epitope tag was precisely knocked-in after the last exon of *VIPP1* in eight of the nine clones (Figure 3c). The precise knocked-in efficiency was 3.2% (8/250; Figure 3d). Using the same screening method, we isolated 10 edited clones at the *IFT46*-gRNA target locus from randomly selected 250 Hm^R colonies with an efficiency of 4% (10/250), and the size of PCR products from three clones was ~400 bp (Figure S3d). Subsequent DNA sequencing confirmed that the *FLAG-HA* tag was precisely knocked-in after the last exon of *IFT46* in all three clones, and the precise knocked-in efficiency was 1.2% (3/250; Figure 3c,d).

The expressions of VIPP1-FLAG-HA and IFT46-FLAG-HA in the precisely edited strains were determined by Western blotting. A 32-kDa VIPP protein was detected in the WT strain and two *IFT46-FLAG-HA* strains using an antibody raised against VIPP1, which was consistent with a previous report (Nordhues et al., 2012). Only one 35-kDa protein was detected in the two *VIPP1-FLAG-HA* strains, which was the expected molecular weight of the VIPP1-FLAG-HA fusion protein, as the predicted molecular weight of the FLAG-HA epitope tag was 3 kDa (Figure 3e). Similarly, one 50-kDa protein was detected in two *IFT46-FLAG-HA* strains, and a 46-kDa IFT46 protein was detected in two *VIPP1-FLAG-HA* strains and the WT strain with an antibody raised against IFT46 (Figure 3e; Hou et al., 2007). Furthermore, when antibodies against FLAG or HA tags were used, bands of approximately 35 kDa in two *VIPP1-FLAG-HA* strains and 50 kDa in two *IFT46-FLAG-HA* strains were detected (Figure 3e), suggesting that the tagged fusion proteins were expressed in these precise knock-in strains.

To determine the subcellular localization of the fusion proteins, the cells expressing the VIPP1-FLAG-HA were stained with antibodies against VIPP1 and HA. The fluorescence signals of VIPP1 and HA were both detected in the chloroplast and were highly merged, which supports the fact that VIPP1 is a chloroplast protein (Figure 3f; Nordhues et al., 2012). The cells expressing IFT46-FLAG-HA were stained with antibodies against IFT46, and the fluorescent signals probed with IFT46 antibody were localized primarily in the basal body and flagella (Figure 3f; Hou et al., 2007; Lv et al., 2017). Similarly, the fluorescence signals probed with the HA antibody were localized primarily in the basal body and flagella, which merged with signals detected by the anti-IFT46 antibody (Figure 3f). Hence, knock-in of the *FLAG-HA* tag did not alter the expression and localization of the endogenous proteins.

Furthermore, we explored this strategy for genes with low-expression levels, such as *CrKU80* and *CrTET1* (Figure S6a,b). At the whole cell population level, the result of nested PCR confirmed that donor DNA was integrated into the Cas9 cut site (Figure S6c). We identified 35 putative edited clones at the *CrKU80*-gRNA4, and 17 at the *CrTET1*-gRNA2 target loci from 200 Hm^R colonies. Sequencing of the targeted region in these clones showed that the *FLAG-HA* tag was precisely knocked-in in the nine clones at *CrKU80*-gRNA4 and five clones at the *CrTET1*-gRNA2 target locus (Figure S6d). The precise knocked-in efficiency was 4.5% (9/200) and 2.5% (5/200) for *CrKU80*-gRNA4 and *CrTET1*-gRNA2 target loci, respectively (Figure S6e).

Collectively, these results demonstrated that the microhomology-mediated short dsDNA donor integration strategy precisely knocked-in the *FLAG-HA* epitope tag in either high-expression genes such as *VIPP1* and *IFT46* or low-expression genes such as *CrKU80* and *CrTET1*.

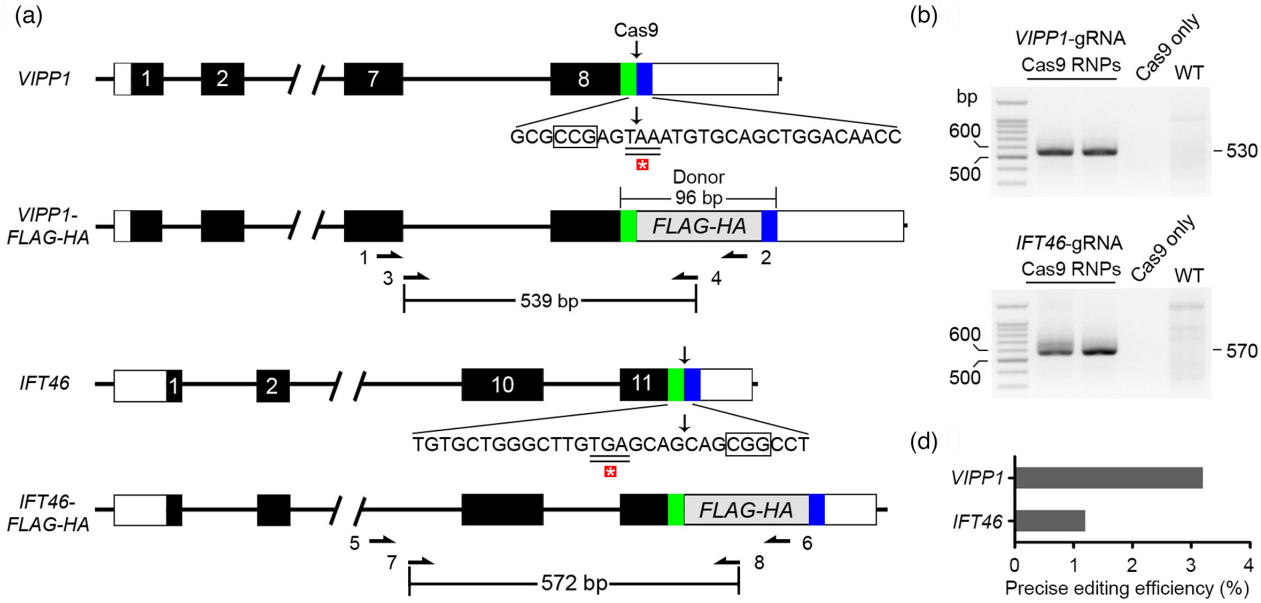

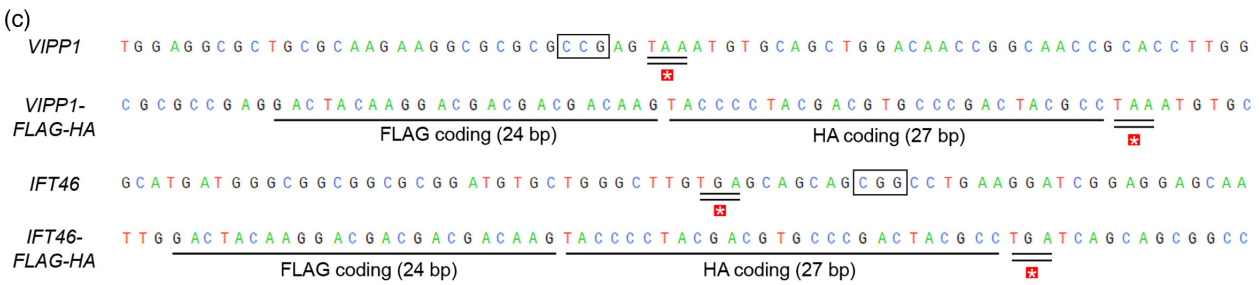

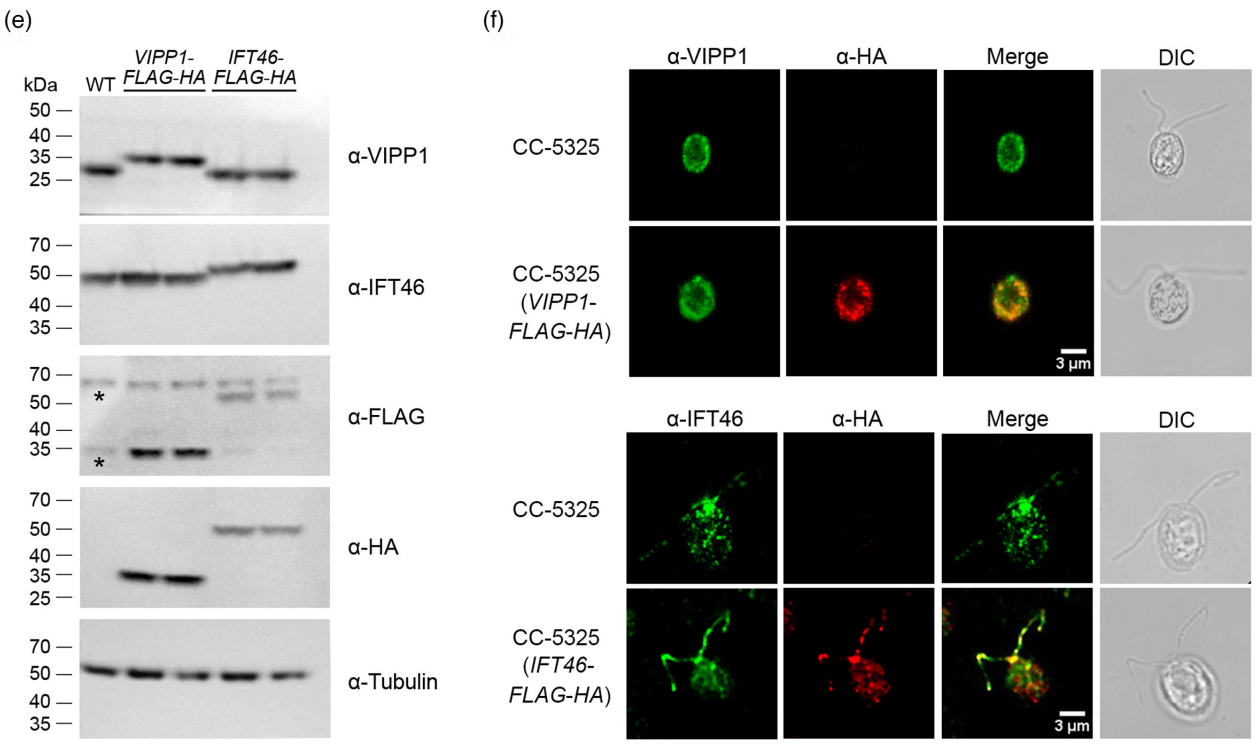

Figure 3. Knock-in of a FLAG-HA epitope tag in the *VIPP1* and *IFT46* genes.
(a) Molecular map of the *VIPP1* locus (Top) and *IFT46* locus (Bottom) with the regions before and after the Cas9 cut site highlighted in green and blue, respectively, as well as the predicted molecular map of the *VIPP1-FLAG-HA* locus (Top) and *IFT46-FLAG-HA* locus (Bottom). Polymerase chain reaction (PCR) with primers 1&2, 3&4, 5&6 and 7&8 can determine whether the donor has been integrated into the Cas9 cut site. The predicted sizes of nested PCR products are indicated. The rectangular box indicates the PAM sequence. The double underline indicates the stop codon.
(b) Confirmation of the donor DNA integrated into *VIPP1*-gRNA/Cas9 (Top) or *IFT46*-gRNA/Cas9 (Bottom) cut site at the cell population level using nested PCR.
(c) DNA sequences of PCR products from the precision-edited clones. A single underline indicates a precisely integrated *FLAG-HA* sequence.
(d) Editing efficiency of *VIPP1* and *IFT46* in 250 randomly selected hygromycin resistance (Hm^R) colonies.
(e) Western blot analysis of whole-cell lysates of CC-5325, two *VIPP1-FLAG-HA* and two *IFT46-FLAG-HA* strains probed with antibodies against VIPP1, IFT46, FLAG and HA epitope peptide. α-Tubulin is the loading control. Note that two weak non-specific bands (*) of approximately 70 kDa and 35 kDa were detected in all samples when antibody against the FLAG epitope peptide was used.
(f) Immunostaining the cells of the *VIPP1-FLAG-HA* strain using antibodies against VIPP1 (green) and HA epitope peptide (red) at Top, and immunostaining the cells of the *IFT46-FLAG-HA* strain using antibodies against IFT46 (green) and HA epitope peptide (red) at Bottom. Differential interference contrast (DIC) images are shown on the right. Scale bar: 3 μm.

Microhomology-mediated knock-in of yellow fluorescent protein (YFP) for live-cell imaging

To further investigate whether microhomology-mediated donor DNA knock-in is also suitable for a high-molecular-weight protein such as fluorescent protein for live-cell imaging, we chose to knock-in the coding region of the YFP protein near the stop codons of *VIPP1* and *IFT46* to create hybrid proteins with YFP at the C-terminus of each gene. This would allow the analysis of target gene expression and the subcellular localization of their gene products in living cells. WT strains (CC-124 and CC-125) and wall-less CC-5325 were used as host strains. An 804-bp DNA donor was designed, and included a 30-bp homologous sequence around the Cas9 cut site on either end, a 714-bp *YFP* coding sequence in the middle, and a 30-bp DNA encoding a flexible linker in front of YFP (Figure 4a; Table S3).

Subsequently, *IFT46* or *VIPP1* Cas9/RNPs, together with donor DNA, and a Pm^R gene expression cassette, were delivered into the CC-5325 or CC-124 and CC-125 strains (Table S1), respectively. To screen potential clones with *YFP* knocked-in, 96 Pm^R colonies were randomly selected and underwent PCR identification. DNA sequencing of PCR products showed that two clones with *YFP* precisely knocked-in were obtained in CC-124, five were obtained in CC-125, and two were obtained in CC-5325 (Figure 4b,c).

The expression of VIPP1-YFP and IFT46-YFP in the precisely edited strains was first determined by Western blotting. A 32-kDa VIPP protein was detected in the CC-124 and CC-125 strains, and a 62-kDa protein was detected in the two *VIPP1-YFP* clones of CC-124 and CC-125 strains when an antibody against VIPP1 was used (Figure 4d), which is the sum of the 32-kDa VIPP and the 30-kDa YFP. Similarly, only a 76-kDa protein was detected in two *IFT46-YFP* clones of the CC-5325 strain, and the 46-kDa IFT46 protein was detected in the WT strain when an antibody against IFT46 was used (Figure 4d). Furthermore, when antibodies against the green fluorescent protein (GFP) tag (which cross-react with YFP tags; Chudakov et al., 2005) were used, the expected tagged proteins were detected (Figure 4d), indicating that VIPP1-YFP and IFT46-YFP fusion proteins were expressed in these knock-in strains.

To determine whether the localization of the fusion proteins represents the subcellular localization of IFT46 and VIPP1, we observed these cells using confocal microscopy and found that the fluorescence signal of *IFT46-YFP* in CC-5325 was specifically found in flagella and basal body as reported (Figure 4e; Lv et al., 2017). The VIPP1-YFP signal in CC-124 or CC-125 was merged with chloroplast autofluorescence (Figure 4f), indicating that VIPP1-YFP was located in chloroplasts as endogenous VIPP1. Furthermore, distinct dot- or rod-like structures of VIPP1 in the chloroplast (Nordhues et al., 2012) was also confirmed. Hence, our method can effectively knock-in a large fluorescent protein at the C-terminus of the protein in multiple *Chlamydomonas* strains.

Use of the modified short homologous arm as donor DNA for precise amino acid substitution

To determine whether the above strategy can be used to substitute a base at specific sites of the target genes, *FLA3* and *FLA10* were selected as the F753L mutation in FLA3 or N329K mutation in FLA10 resulted in flagella disassembly at restrictive temperatures (Mueller et al., 2004; Vashishtha et al., 1996). Amino acid substitutions at a specific site often require only one base change, making it difficult to screen precisely edited candidate clones through PCR amplification. To overcome this issue, we selected the target loci of gRNA in the intron adjacent to the exon in which a base substitution was intended. An exogenous 38-bp fragment was included in the donor DNA and flanked by 154–200-bp homologous arms, which included the site requiring base substitution (Tables S1 and S3). In theory, the precisely edited mutant obtained by this strategy would not only achieve base replacement but also contain an insert of 38 bp in the intron adjacent to the Cas9 cut site. The 38-bp insertion allowed the detection of donor integration using PCR based on the size change of the PCR products.

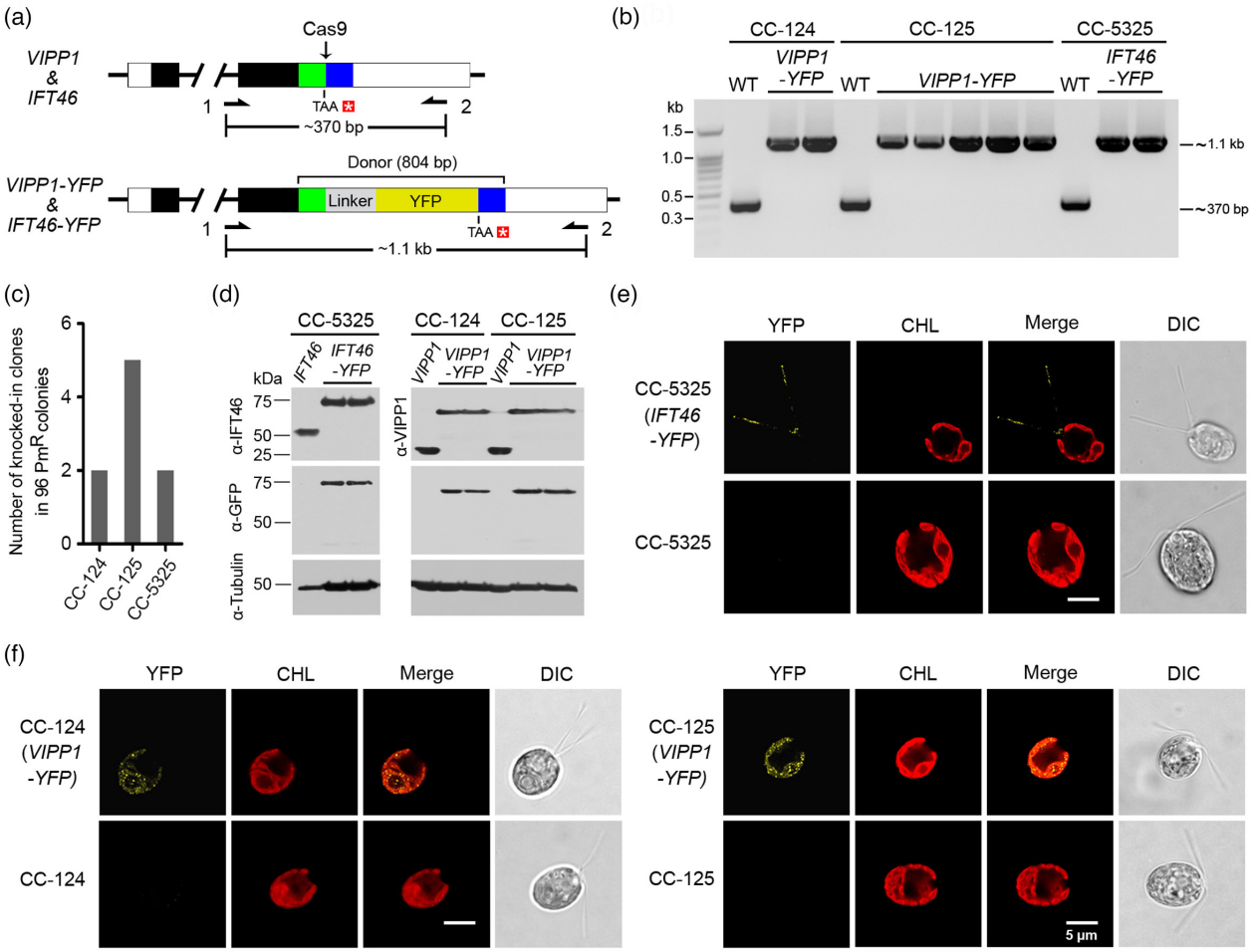

Figure 4. Microhomology-mediated knock-in of the yellow fluorescence protein (YFP) gene in multiple *Chlamydomonas* strains for live-cell imaging.
(a) Top: Molecular map of the *VIPP1* and *IFT46* loci with the Cas9 cut site. Bottom: Predicted molecular map of the *VIPP1-YFP* and *IFT46-YFP* loci with the integration of the donor containing a flexible linker (gray rectangle) and YFP (yellow rectangle) at the Cas9 cut site. Polymerase chain reaction (PCR) with primers 1 and 2 can amplify the genomic sequence containing the gRNA target site, and the predicted product size is either ~370 bp from wild-type (WT) or ~1.1 kb after integration of *YFP*. The asterisk indicates the stop codon. Green and blue colors highlight the genomic regions before and after the Cas9 cut site, respectively.
(b) The putative precision-edited mutants were identified from 96 randomly selected hygromycin resistance (Hm^R) colonies of CC-124 or CC-125, or CC-5325 strains, respectively.
(c) The number of knocked-in clones was calculated from randomly selected 96 Hm^R colonies.
(d) Left: Western blot analysis of whole-cell lysates of CC-5325 and two *IFT46-YFP* strains probed with antibodies against IFT46 and GFP. Right: Western blot analysis of whole-cell lysates of CC-124 and CC-125, and two *VIPP1-YFP* strains probed with antibodies against VIPP1 and GFP. α-Tubulin was the loading control.
(e) Live-imaging of IFT46-YFP in CC-5325 strain expressing the IFT46-YFP fusion protein. Differential interference contrast (DIC) images were shown on the right.
(f) Live-imaging of VIPP1-YFP in CC-124 (left) and CC-125 (right) strains. CHL, chlorophyll. Scale bar: 5 μm.

The codon TTC encoding phenylalanine Phe753 of FLA3 was in exon 17; therefore, the target locus of *FLA3*-gRNA was selected on intron 17. The first base T of the codon TTC, substituted by C, was introduced into the left homologous arm (Figure 5a). Using the same principle, we designed a repair template to substitute the last base C of the codon AAC encoding Asn329 of FLA10 (Figure 5a). Nested PCR confirmed that donor DNA was integrated into the Cas9 cut site in *FLA3* or *FLA10* at the cell population level in the host strain CC-5325 (Figure S7a,b).

To identify the clones that were edited at the *FLA3*-gRNA target locus, 250 Hm^R colonies were randomly selected, and PCR products of different sizes compared with the WT cells were obtained from 16 clones, including eight putative precision-edited clones (Figure S3e). Sequencing of these PCR products confirmed that seven of eight clones had T to C substitution at the first base of the codon at amino acid 753 of FLA3, and the exogenous 38-bp DNA fragment was precisely integrated at the Cas9 cut site in intron 17 (Figure 5b). Using a similar strategy, we isolated 10 clones edited at the *FLA10*-gRNA target locus from 250 randomly selected Hm^R colonies (Figure S3f). Four clones had A to C substitution at the third base of the codon AAC encoding amino acid 329 of FLA10 (Figure 5b). In summary,

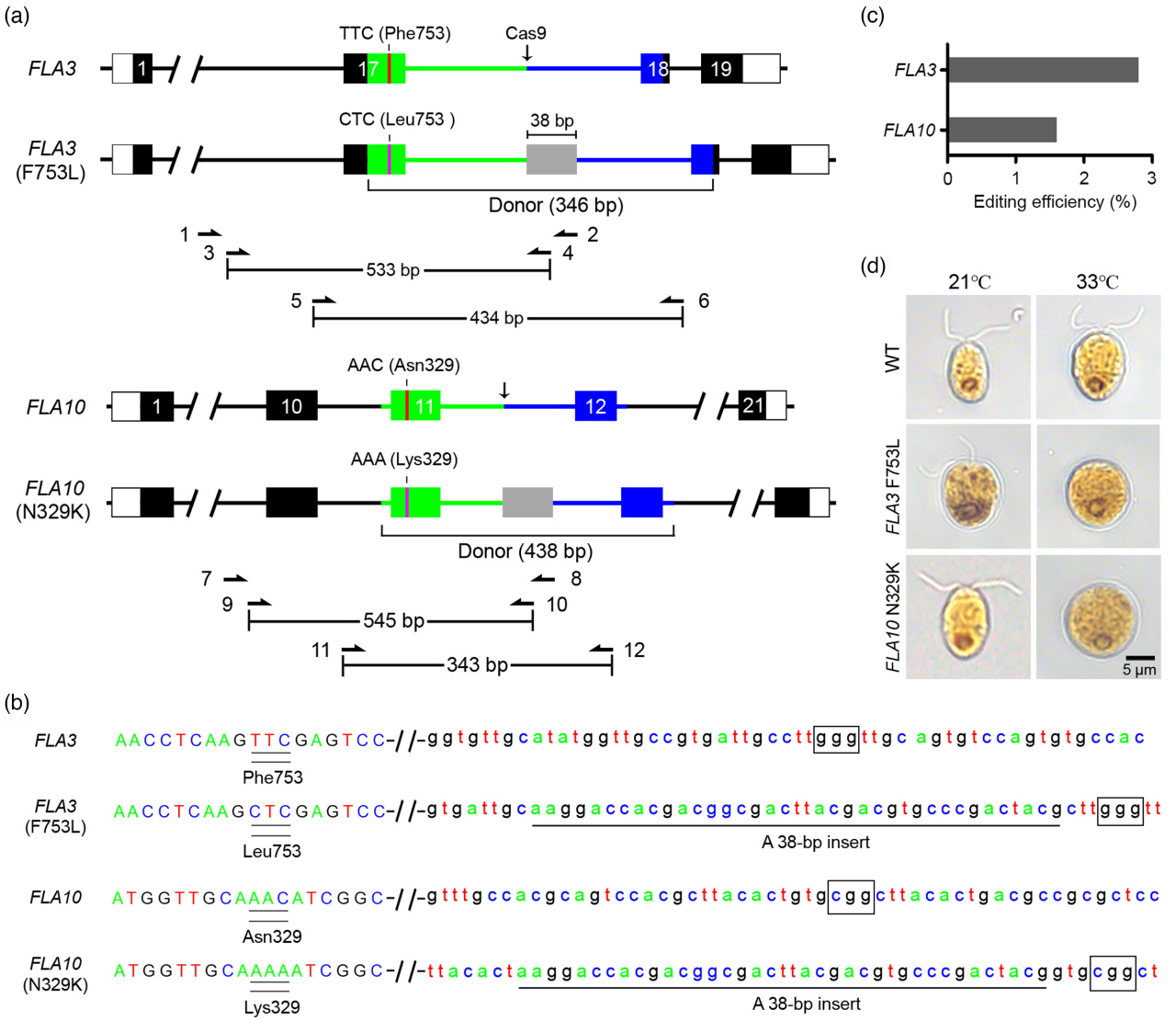

Figure 5. Precise substitution of amino acids for the *FLA3* and *FLA10* genes.
(a) Strategy for generating amino acid substitution mutants using a donor with two short homologous arms, with the left one (green) containing the substituted base (vertical line). A 38-bp exogeneous sequence (gray) is included between the left (green) and right (blue) arms for integration into an intron to facilitate polymerase chain reaction (PCR) screening. Primers are indicated with the expected product sizes.
(b) Sequence of the edited *FLA3* and *FLA10* genes. The mutated codons are double-underlined. The 38-bp fragment (underlined) is precisely integrated at the Cas9 cut site. The PAM site is boxed.
(c) Editing efficiency of *FLA3* and *FLA10* in 250 randomly selected hygromycin resistance (Hm^R) colonies.
(d) Flagellar assembly at the permissive temperature and disassembly at the non-permissive temperature in the edited strains. Scale bar: 5 μm.

the precise-editing efficiency was 2.8% (7/250) for *FLA3*-gRNA, and 1.6% (4/250) for *FLA10*-gRNA (Figure 5c).

Moreover, we confirmed that the 38-bp endogenous DNA fragment integrated into the intron had no effect on the transcription and maturation of *FLA3* and *FLA10* mRNA (Figure S7c–e). The flagellar phenotypes of the isolated *FLA3* F753L and *FLA10* N329K strains were analyzed. The flagellum of *FLA3* F753L cells was shorter than that of the WT cells, whereas *FLA10* N329K cells showed no difference when the cells were cultured at 21°C (Figure S8a). Consistent with a previous report (Mueller et al., 2004), the flagella of *FLA3* F753L and *FLA10* N329K cells disassembled when cells were cultured at 33°C (Figures 5d and S8b).

To exclude the locus-specific effect of the above results, we selected *FTSY* as the third target gene in another strain CC-1328. A 360-bp dsDNA was designed as a repair template, including a 38-bp exogenous DNA in the middle and 161-bp short-homologous arms at each flank (Table S1). The first base G of the codon GAG encoding Glu290 on the right homologous arm was replaced by T, resulting in a stop codon (Figure S9a). Twenty-three light-green colonies were obtained from two plates 10 days

after electroporation (Figures S9b and S5b). Amplification of the target region and sequencing of the PCR products showed that the target sites were edited in all 23 light-green clones, among which the size of PCR products from seven clones was ~670 bp (Figure S3h). DNA sequencing of these PCR products revealed that five of seven clones had G to T substitution at the codon encoding Glu290 (Figure S9c). The efficiency of precise amino acid substitution at the target site of *FTSY*-gRNA2 was 1.5% (5/326; Figure S9d). These results indicated that the modified short-homologous arm mediated donor DNA integration strategy could be used to produce base substitutions at most, if not all, sites in a target gene.

Micro-homologous donor mediated precise deletion of the 3′-UTR of *MAA7* and *VIPP1*

To assess whether our method can be applied to delete a DNA fragment such as the 3′-UTR of a target gene for stable knock-down, we selected *MAA7* to test. The inhibition of *MAA7* expression resulted in resistance to 5-FI in *Chlamydomonas* (Zhao et al., 2009), which would facilitate the screening for knock-down clones. We chose two gRNA targets located at the 5′- and 3′-terminals of the 474-bp *MAA7* 3′-UTR, gRNA1 and gRNA2 (Figure S10a). Assuming that the addition of a donor may favor accurate repair of a DSB, we designed a 98-bp sequence as a homologous donor template for the two respective gRNA target sites (Figure S10a).

MAA7 Cas9/RNPs together with donor DNA, only Cas9/RNPs or only donor DNA were electroporated into *Chlamydomonas* cells CC-5325. More than 100 5-FI-resistant colonies were obtained in the Cas9/RNPs + donor group, whereas only seven were obtained in the donor-only group, and only four in the Cas9/RNPs-only group (Figure S10b). The last two types of 5-FI-resistant mutants may result from the mutations of two other genes, *MAA2* and *TAR1* (Palombella & Dutcher, 1998), or NHEJ-mediated imprecise editing at the gRNA1 or gRNA2 locus of *MAA7*.

We randomly selected 96 5-FI-resistant colonies from the *MAA7* RNPs + donor group, and obtained PCR products covering the *MAA7* 3′-UTR. The PCR products of 18 clones were ~300 bp, which may have been generated from the precise deletion of the 3′-UTR, and integration of the 98-bp DNA donor (Figures S10a,c and S11a). Subsequently, DNA sequencing showed that the DNA fragment between the two Cas9 cut sites was precisely deleted in seven clones, while another nine clones were precisely deleted and integrated with the donor DNA (Figures S10d and S11b). In addition to the deletion mutants, 73 insertion-only mutants were obtained from 96 5-FI-resistant colonies. Among 30 randomly selected clones, the donor DNA was inserted at the gRNA2 target locus in 24 clones, was inserted into two gRNA loci in four clones, and was inserted in the gRNA1 locus in two clones (Figures S10c,e and S11a).

To investigate whether stable knock-down of the expression of *MAA7* was achieved, we examined transcription levels of *MAA7* in two clones with precise deletions, two clones with precise deletions plus donor DNA integration, and four clones with donor DNA insertion-only at gRNA2 target locus cultured in TAP medium without 5-FI in 1 or 2 months. The transcription level of *MAA7* was reduced by 75–90% in four deletion clones, and by 50–60% in four insertion-only clones compared with the WT cells (Figure S10f). Spot growth assay showed that the growth rate of all selected mutants was slower than that of the WT (Figure S10g), and the growth rate of deletion clones was slower than that of insertion-only type clones on TAP-agar plates with 20 μM 5-FI (Figure S10g), which correlated well with the knock-down level of *MAA7* (Figure S10f).

To further determine the feasibility of this DNA fragment deletion method without pre-screening the mutant based on the altered phenotype, we selected *VIPP1* as an example. The strategy for precisely deleting the 3′-UTR of *VIPP1* was similar to that for *MAA7* 3′-UTR (Figure 6a), except that the Pm^R cassette was included in the electroporation for obtaining putative edited clones (Table S1). We electroporated *VIPP1* Cas9/RNPs + donor + Pm^R, *VIPP1* Cas9/RNPs + Pm^R, and *VIPP1* Cas9/RNPs + donor into CC-5325 cells, respectively. We obtained a similar number of clones in the *VIPP1* RNPs + donor + Pm^R and *VIPP1* RNPs + Pm^R group, and no resistant clones were obtained in the *VIPP1* RNPs + donor group as expected (Figure S12a).

Ninety-six Pm^R colonies from the *VIPP1* RNPs + donor + Pm^R group were selected, and the 3′-UTR region was amplified and sequenced. The PCR products of six clones were ~400 bp as expected, including three clones (designated a1–a3) with the 3′-UTR deleted plus precise donor integration, and three clones (designated b1–b3) with the 3′-UTR deleted plus imprecise donor integration between the two Cas9 cut sites (Figures 6b,c and S12b,c). PCR products from 10 clones were slightly larger than the WT (Figures 6b and S12b), indicating that the donor inserted into one or both of the gRNA sites. PCR products of eight clones were significantly larger than WT (Figures 6b and S12b), resulting from unexpected insertion of the whole Pm^R cassette or part of the cassette. In the *VIPP1* Cas9/RNPs + Pm^R group, we identified only nine clones in which the intact Pm^R cassettes or the fragments of the cassettes were integrated into the gRNA target locus in 96 Pm^R clones, but did not obtain the clones in which deletion of 3′-UTR between two gRNA target loci occurred (Figure 6b). These results suggested that donor DNA with micro-homologous arms is crucial in the repair of the two DSBs.

To investigate whether stable knock-down of VIPP1 was achieved, we examined transcription levels of *VIPP1* in two clones (a1 and a2) with the 3′-UTR deleted plus precise donor integration, and two clones (b1 and b2) with the 3′-UTR deleted plus imprecise donor integration after 1 or

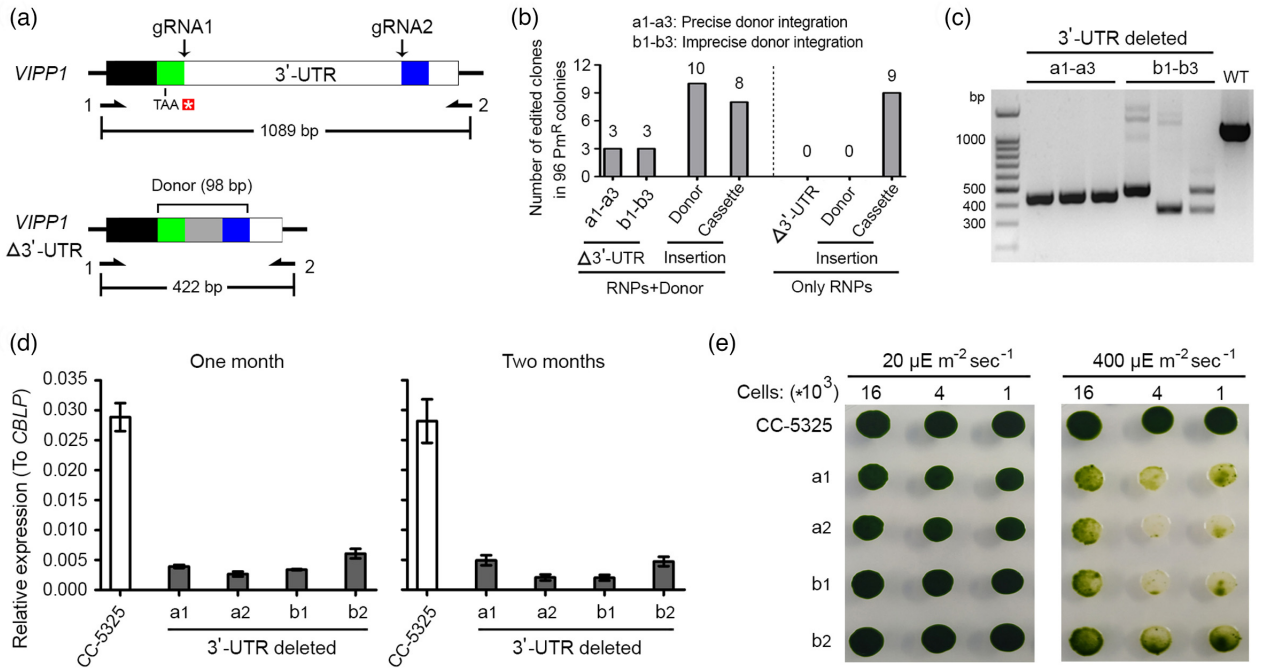

Figure 6. Stable knock-down of *VIPP1* through microhomology-mediated deletion of a DNA fragment encoding its 3′-UTR.
(a) Top: Strategy for deleting a DNA fragment in the 3′-UTR of *VIPP1* using two 685-bp apart sgRNA target sites. The asterisk indicates the TAA stop codon of *VIPP1*. Bottom: Diagram of the precise editing showing deletion 3′-UTR with an insertion of the 98-bp donor containing a 38-bp intervening sequence (gray box). Green and blue colors highlight the 30-bp micro-homologous arms of the genomic sequences before the sgRNA1 and after the sgRNA2 binding sites, respectively. Polymerase chain reaction (PCR) with primers 1 and 2 can amplify the genomic sequence covering the two gRNA target loci, with products of indicated size.
(b) The mutant types among 96 paromomycin resistance (Pm^R) colonies generating from transformation with ribonucleoproteins (RNPs) + Donor and among the 96 Pm^R colonies from RNPs-only transformation. Donor denotes the clones containing donor insertion at a gRNA site but without the deletion of the UTR. Cassette denotes the clones with the DNA fragment conferring Pm^R detected to be inserted at the gRNA target sites.
(c) PCR results of three deletion plus precise donor integration mutants (a1–a3) and three deletion plus imprecise donor integration mutants (b1–b3) obtained from transformation using both RNPs and donor.
(d) mRNA levels of *VIPP1* in the mutants of a1, a2, b1, b2 and the wild-type (WT) cells upon 1 month (left) and 2 months (right) of continuous growth on plates, respectively. Reverse transcription-quantitative polymerase chain reaction (RT-qPCR) was performed independently three times in triplicate. Data are represented as mean ± standard error (SE).
(e) Spot test for growth of the WT strain, and the mutants of a1, a2, b1, b2 under indicated light intensities.

2 months of culture. The transcription level of *VIPP1* was reduced by 80–90% compared with that in WT cells in the four clones with the 3′-UTR deleted (Figure 6d). The growth of these four clones had no difference compared with WT under the normal light conditions in 2 months (Figure 6e), but they showed obvious photobleaching phenotype under the high light conditions (Figure 6e), consistent with previous reports (Hu et al., 2014; Nordhues et al., 2012). The above results demonstrate that HDR of two cut sites facilitates effective fragment deletion from a 3′-UTR, enabling the investigation of essential genes by evaluating knock-down effects in *Chlamydomonas*.

DISCUSSION

In this study, we established a multi-type precision gene-editing approach using a microhomology-mediated donor integration-dependent screening pipeline to isolate the knock-out, knock-in and knock-down mutants in *Chlamydomonas*. The main steps of this approach included rational donor design, partial optimization of targeting strategies according to different gene-editing purposes, generation of drug-resistant co-transformants, PCR screening and functional verification. We increased the overall efficiency of genome editing by selecting the gRNA targeting site and shortening the DNA donor, primarily using micro-homologous donor DNA. The donor DNA containing micro-homologous arms may not only be involved in HR-dependent precise editing (Hockemeyer et al., 2011; Yang et al., 2013), but rather can also be precisely knocked-in through MMEJ-mediated donor DNA integration (Bae et al., 2014; Sakuma et al., 2016). Therefore, donor DNA integration can be achieved through these two pathways, increasing the probability of precise editing at the gRNA target locus. Furthermore, our approach to precision editing has two advantages. First, we set up a checkpoint to determine whether the donor DNA integration occurs at the target locus in the whole cell population, which ensures that the cell pool used for further screening

contains the cells with donor integration at the gRNA target locus. This checkpoint can also be used to compare the relative efficiency of the gRNA targets. Another checkpoint in the pipeline ensures that the screening of a large number of putative clones becomes feasible, which is helpful for low-expression genes. Second, adding a short exogenous DNA sequence in an intron did not alter the expression of the target gene, but greatly facilitated the screening of a point mutation using PCR. Making use of these approaches, we investigated four scenarios, including targeted gene inactivation, single amino acid substitution, knock-in of an epitope or a YFP tag, and precise deletion of specific sequences (illustrated in Figure S13).

This study demonstrated that the gene-editing efficiency mediated by Cas9-gRNA RNPs is positively correlated with the transcriptional level of genes in *Chlamydomonas*. The genes with high-expression levels typically have an open chromatin structure (Li et al., 2004), which increases the accessibility (Jiang & Pugh, 2009) and binding of the Cas9/gRNA RNP complex to the target site (Jensen et al., 2017). Conversely, the dense chromatin structure of genes with lower expression often hinders or reduces the accessibility and binding of DNA-binding proteins to the target site (Chereji et al., 2016). Therefore, the cleavage efficiency of the RNP complex on the genes with high expression is greater than that on genes with low expression, corresponding directly to higher gene-editing efficiency.

When an equal number of long or short donor DNA was used as the repair template, the editing efficiency was found to be higher with the short donor DNA. This might have been due to the smaller short donor DNA being more efficiently delivered into the cells during electroporation, while the longer donor DNA is apt to be digested by DNase in the cells of *Chlamydomonas* (Zhang et al., 2014). Alternatively, the long and short DNA donors may have different roles in DSB repair. That is, the long DNA donor may mediate HR-dependent illegitimate recombination, while the integration of short donor DNA might participate in the MMEJ pathway, in which exogenous DNA fragments can be integrated into the genome without base deletion at the junction site (Sakuma et al., 2016; Yao et al., 2017). The MMEJ pathway reportedly plays a predominant role in the repair of CRISPR/Cas9-induced DSBs in *Chlamydomonas* (Sizova et al., 2021).

We demonstrated precise knock-in of a stop codon or an epitope/YFP tag in two low-expression genes *CrTET1* and *CrKU80* using donor DNA with micro-homologous arms. Supplying donor DNA containing micro-homologous arms increased the editing efficiency over the methods resorting to NHEJ-dependent editing as used previously for the *CrTET1* gene (Xue et al., 2019). So the mutants with donor integration at the Cas9 cut site could be identified directly from randomly selected antibiotic-resistant colonies for the genes with the expression level exceeding 5 (FPKM value; Figure 1). This allowed us to analyze mutants for multiple loci in the same target gene to determine their common phenotypes, while simultaneously circumventing the concern of off-target effects resulting from random insertion of the donor DNA in the genome. In addition, donor DNA with micro-homologous arms was suitable for precise knock-in of epitope tags into the target gene coding sequence as the tag is generally a peptide encoded by a short DNA sequence. Given that the position of the epitope tag knock-in within a given gene is fixed, the selection of a useful gRNA target site is often limited, and the selected target site might not exhibit optimal editing efficiency. The increase in the editing efficiency with the donor DNA can compensate for this loss, resulting in substantially higher efficiency of gene knock-out and tag knock-in (Figures 2, 3 and S6).

Furthermore, amino acid substitution was successfully achieved at specific sites of *FLA3* and *FLA10* with an efficacy of 2.8% and 1.6%, respectively (Figure 5). Considering that amino acid substitution at a specific site typically requires altering a single or several bases, screening for the putative edited clones based on PCR product size was difficult. In our approach, the target locus of gRNA was selected in the intron adjacent to the exon where the base substitution was intended, and the micro-homologous arms were replaced with 150–200-bp short-homologous arms in which the sites requiring base substitution were included. Additionally, a 38-bp exogenous DNA fragment was inserted in the middle of the donor DNA, which was designed to detect whether the donor DNA was integrated into the gRNA target locus and facilitated the screening of putative edited colonies. Our data showed that inserting a 38-bp fragment into an intron did not affect the transcription of the target genes in *Chlamydomonas* (Figure S7). This strategy expanded the selection range of the optional gRNA targets within the gene of interest, increasing the screening efficiency for precise amino acid substitution. Hence, mutants with a single amino acid change in the protein can be used to confirm the active site of an enzyme and a protein–protein interaction site in *Chlamydomonas*.

This study is also the first to achieve microhomology-mediated precise DNA fragment deletion in *Chlamydomonas*. Deleting the 3′-UTR fragment of *MAA7* and *VIPP1* resulted in stable knock-down of their expression over the 2-month test period (Figures 6d and S10f). This method circumvents the need for artificial MicroRNAs, which often become gradually silenced by epigenetic regulation (Hu et al., 2014). We also found that adding a micro-homologous donor DNA as a template for DSB repair was beneficial in DNA fragment deletion between two gRNA loci. More than 50% of the clones with fragment deletion of *MAA7* or *VIPP1* 3′-UTR were precisely integrated with donor DNA. This is notable as CRISPR/Cas9-mediated DNA

deletion theoretically requires simultaneous cutting at both gRNA loci and relies on the NHEJ pathway to complete the repair of both DSBs. This NHEJ-based repair process does not require donor DNA in human and *Arabidopsis thaliana* cells (Li et al., 2018; Liu et al., 2016). We were unable to obtain clones with fragment deletion without providing micro-homologous donor DNA for the two gRNA loci on the target gene 3′-UTR (Figures 6b and S10b), which may indicate that both NHEJ and MMEJ pathways have a high preference for integrating exogenous DNA during DSB repair in *Chlamydomonas*. Hence, when microhomology or short homology arms were added to exogenous DNA, the homology-containing donor may have facilitated the occurrence of precise repair events by HR.

The precise deletion of DNA fragments required targeting two gRNA loci on 3′-UTR. As expected, we obtained complete deletion as well as insertion type clones in which the donor DNA integrated at one gRNA locus (Figures 6b,c and S10c,e). We also found that inserting donor DNA into the 3′-terminus of the 3′-UTR resulted in reduced expression of the target genes. More specifically, target gene expression was reduced by 80–90% in the complete deletion-type clones and by 50–60% in the insertion-type clones compared with WT cells. This may indicate that the knock-down effects of the two editing types of clones result from different mechanisms. According to a recent report (Zhao, Siegel, et al., 2017; Zhao, Steinfeld, et al., 2017), clones with DNA fragment deletion of 3′-UTR may reduce both the initial abundance of mature mRNA at the transcriptional level and the stability of mature mRNA at the post-transcriptional level. Hence, the insertion of donor DNA at the 3′-end of the 3′-UTR might have only affected the stability of mature mRNA at the post-transcriptional level. These two types of clones with different knock-down effects can also be used to study gene expression dose-dependent phenotypes. In addition, this fragment deletion strategy can also be applied to the generation of truncated proteins, which can be used to explore the regulatory mechanism and function of different protein isoforms and verify the function of promoters and enhancers in *Chlamydomonas*.

To compare the precision-editing efficiency in this study with that in previous publications, two representative works such as knocked-in of a Flag (Greiner et al., 2017) and a 6xHis tag (Ferenczi et al., 2017) in the exons of target genes were used (Table 1). The efficiency of precision knock-in a Flag tag on exons of different target genes was 0–2 clones out of the 96 co-selection resistance clones (Greiner et al., 2017; Table 1). In our method, the precision knock-in efficiency of a 3xStop codons donor DNA in exons of different target genes was 1.4–6%, and those of a FLAG-HA tag or YFP tag near the stop codon (restricted position) for several target genes were 1.2–4.5% and 2–5 clones out of the 96 identified resistance clones (Table 1). In contrast, Ferenczi et al. (2017) reported an editing efficiency for the precise knock-in of 3xStop codons donor and 6xHIS tag of up to 40%, which was due to the FKB12-edited mutant gaining rapamycin resistance (Table 1). However, for *FTSY*, *SRP43* and *PHT7*, in which no phenotypic or antibiotic resistance screening was used, the efficiency of precision knock-in 3xStop codons donor dropped to 0.25%, 0.12% and 8.2%, respectively (Table 1).

The precision knock-in efficiency was also compared with previously published studies using the same target genes (*CrKU80* and *FTSY*). In the report by Greiner et al. (2017), no precision Flag knock-in clone in the exon of *CrKU80* was obtained from 96 co-selection clones (Table 1), while one clone exhibited imprecise Flag tag knock-in (Table S2). Using our method, the precision knock-in efficiency of donor DNA in three different *CrKU80* exons reached 2%, 6% and 3% (Table 1); the efficiency of imprecise editing was 8%, 22% and 9% (Table S2). Regarding the target site limited to the stop codon, the precision knock-in efficiency of the FLAG-HA tag in *CrKU80* also reached 4.5% (Table 1). For *FTSY*, the precision-editing efficiency in Ferenczi et al.'s (2017) study was 0.25%, while that in the current study was 1.4% (Table 1). Hence, our approach improves precision-editing efficiency in terms of multiple target genes and two genes at a specific target site. We also found that the precise-editing efficiency is highly correlated with that of imprecise gene editing (Figure 2), which can be used to generate knock-out mutants. That is, the total efficiency of gene editing is highly dependent on the recipient strains and target genes (Table S2).

Our results also confirmed that the resistance expression cassette was integrated into gRNA target sites by the NHEJ pathway in a portion of the clones, as reported by Jeong et al. (Shin et al., 2016). The generation of this type of off-target mutation primarily resulted from the formation of DSBs induced by cutting the DNA at the target sites with the gRNA/Cas9 RNP complex. In addition, the resistance expression cassette was randomly integrated into the genome when shorter donor DNA was co-delivered with an antibiotic resistance gene, resulting in a second type of off-target mutation. To avoid this, the obtained mutant can be crossed with WT cells to remove the off-target mutation in different chromosomes. In addition, the WT gene can be introduced to rescue the mutant phenotype. Indeed, these methods are well-developed strategies to rule out the off-target mutations in *Chlamydomonas*.

In summary, we provided comprehensive protocols for gene editing in *C. reinhardtii*. The methods described result in knock-out mutants of low-expression genes, precise knock-in of tags into a coding sequence, amino acid substitution at a specific site, or deletion of a DNA fragment in the genome and simultaneous generation of double mutants. Hence, this study provides a novel means to achieve genetic modification in *Chlamydomonas*.

Table 1 Comparison of the precision-editing efficiency using the method presented in this study with that in the two recent publications

Targeted gene inactivation (knock-in FLAG tag into the exon)		Amino acid substitution		Precise deletion of DNA fragments		
Target gene	Efficiency	Target gene	Efficiency	Target gene	Efficiency	Reference
aCRY	0 out of 96	No application		No application		Greiner et al. (2017)
COP1/2	0 out of 96					
UVR8	0 out of 96					
COP5	1 out of 96					
VGCC	0 out of 96					
CrKU80	0 out of 96					
POLQ	0 out of 96					
MAT3	2 out of 96					
PHOT	2 out of 96					

Targeted gene inactivation (knock-in 3xStop codons into the exon)		Knock-in 6xHis-1xStop codon into the exon		Amino acid substitution		Precise deletion of DNA fragments		
Target gene	Efficiency	Target gene	Efficiency	Target gene	Efficiency	Target gene	Efficiency	Reference
FKB12	40%	*FKB12*	3 out of 6	No application		No application		Ferenczi et al. (2017) (Phenotypic screening)
FTSY	0.25%							
SRP43	0.12%							
PHT7	8.2%							

Targeted gene inactivation (knock-in 3xStop codons into the exon)		Knock-in a FLAG-HA epitope or YFP tag at the C-terminal of the protein		Amino acid substitution		Precise deletion of DNA fragments		
Target gene	Efficiency	Target gene	Efficiency	Target gene	Efficiency	Target gene	Efficiency	Reference
CrKU80	2% for gRNA1	*VIPP1*	3.2%	*FLA3*	2.8%	*MAA7*	16 out of 96	In this study
	6% for gRNA2	*IFT46*	1.2%					
	3% for gRNA3	*CrTET1*	2.5%	*FLA10*	1.6%			
FTSY	1.4%	*CrKU80*	4.5%			*VIPP1*	3 out of 96	
		VIPP1 (YFP)	2 out of 96 (CC-124) 5 out of 96 (CC-125)	*FTSY*	1.5%			
		IFT46 (YFP)	2 out of 96					

EXPERIMENTAL PROCEDURES

Expression and purification of *Streptococcus pyogenes* Cas9 (SpCas9)

The DNA encoding SpCas9 was cloned into the pPEI-His-SUMO vector with *Bam*HI and *Xho*I. The plasmid pPEI-His-SUMO-SpCas9 was transformed into the *Escherichia coli* strain *Transetta* (DE3; TransGen, Beijing, China). The transformants were grown in 2xYT medium with kanamycin (50 mg ml^{-1}) and chloramphenicol (34 mg ml^{-1}) at 37°C until the OD_{600} reached 0.6, and then incubated at 16°C for 16 h with 0.2 mM of isopropyl-β-D-thiogalactopyranoside (IPTG; Sangon Biotech, Shanghai, China) to induce the expression of SpCas9. Cells were harvested and resuspended in lysis buffer [20 mM Tris–HCl, pH 8.0, 500 mM NaCl, 5 mM imidazole, 1 mM dithiothreitol (DTT) and 1 mM PMSF] and then broken using the UH-03 homogenizer (Union Biotech, Hangzhou, China) under a pressure of 800 bar. The lysate was centrifuged at 15 000 ***g*** for 1 h (Beckman Coulter, Brea, CA, USA), and the supernatant was incubated with Ni-NTA resin (Qiagen, Venlo, The Netherlands) for 1 h. The resin was filled in a gravity-flow column (Bio-Rad, Hercules, CA, USA) and washed with 10 column volumes of washing buffer (20 mM Tris–HCl, pH 8.0, 500 mM NaCl, 20 mM imidazole and 1 mM DTT). The ULP1 peptidase was added to the washed resin and incubated for 15 h. The cleaved SpCas9 was eluted from the resin with elution buffer (20 mM HEPES, pH 7.5, 100 mM KCl, 1 mM DTT and 10% glycerol). The eluted protein was loaded into a 5-ml HiTrap SP HP Sepharose column (GE Healthcare Life Sciences, Pittsburgh, PA, USA) and eluted in buffer A (20 mM HEPES pH 7.5, 100 mM KCl, 1 mM DTT and 10% glycerol) with a linear gradient from 100 mM to 1 M KCl. The protein was concentrated into 500 μl using a centrifugal filter (30 kDa, Millipore, Billerica, MA, USA), and further purified by gel filtration on a Superdex 200 10/300 column (GE Healthcare Life Sciences) in GF buffer (20 mM HEPES pH 7.5, 150 mM KCl, 1 mM DTT and 10% glycerol). The eluted protein was quantified with sodium dodecyl sulfate–polyacrylamide gel electrophoresis (SDS–PAGE) and passed through a 0.2-μm filter (Whatman, Maidstone, UK) to

remove potential bacteria contamination from the purified protein. The filtered protein was concentrated to ~20 mg ml^{-1} with a clean centrifugal filter (30 kDa, Millipore), flash-frozen in liquid nitrogen, and stored at −80°C.

In vitro transcription and functional verification of single-guide RNAs (gRNAs)

The gRNAs targeting the *CrKU80*, *CrTET1*, *FKB12*, *VIPP1*, *IFT46*, *FLA3*, *FLA10* and *FTSY* genes in *C. reinhardtii* were designed using CRISPR RGEN Tools (http://www.rgenome.net/cas-designer/). The gRNAs targeting the *MAA7* were referred to the previous publications (Xue et al., 2019). The gRNA was transcribed *in vitro* using the HiScribe™ T7 Quick High Yield RNA Synthesis Kit (NEB, Ipswich, MA, USA). Transcribed RNA was purified using Monarch® RNA Cleanup Kit (NEB). Purified gRNAs for each target loci were quantified using NanoDrop 1000 spectrophotometer (Thermo Scientific, Waltham, MA, USA). The activities of the gRNAs and the Cas9 protein were verified *in vitro* before their use *in vivo*. The genomic DNA was extracted from *C. reinhardtii* using TransDirect Plant Tissue PCR Kit (Transgen). The template DNAs encompassing the Cas9 cut site were amplified using Gflex high-fidelity DNA polymerase (Takara, Shiga, Japan). For *in vitro* assays, 700 ng purified Cas9 was pre-incubated with 500 ng gRNA in Cas9 cleavage buffer (20 mM HEPES, pH 7.5, 100 mM NaCl, 5 mM $MgCl_2$, 0.5 mM DTT, 0.1 mM EDTA) at 37°C for 30 min, then 500 ng template was added, and the mixtures were incubated at 37°C for 30 min, then 10×STOP solution (0.5 M EDTA, 80% glycerol and 10% SDS) was added. The final products were separated using 2% agarose gel electrophoresis and imaged on a UVP BioDoc-It system. All the sequences of gRNA and primers were shown in Table S3.

Chlamydomonas reinhardtii strains and culture conditions

The walled *C. reinhardtii* strains CC-124, CC-125, CC-1328, and the wall-less strain, CC-5325, were obtained from the Chlamydomonas Resource Center at the University of Minnesota (http://www.chlamycollection.org). All strains were cultured mixotrophically in TAP medium on a rotary shaker at 25°C and maintained at a light intensity of 20 μmol photons m^{-2} sec^{-1} (Gorman & Levine, 1965).

Preparation of dsDNA donors containing micro-homologous arms for targeting *CrKU80, CrTET1, VIPP1, IFT46, FLA3, FLA10, MAA7* and *FTSY*

To construct a long dsDNA donor for targeting *CrTET1* and *CrKU80*, the 25-bp micro-homologous arm to the flank sequence of the Cas9 cleavage site of *CrTET1*-gRNA or *CrKU80*-gRNA1 was added to both sides of the expressing cassette of hygromycin including the *TUBULIN2* promoter, *APHVII* or *APHVIII* coding sequence, and *RBCS2* terminator (Cheng et al., 2017) by using specific forward and reverse primers containing 25-bp micro-homologous arms, respectively. To construct dsDNA donor for knock-in YFP tag after *VIPP1* and *IFT46* coding sequence, the 25-bp micro-homologous arm to the flank sequence of the Cas9 cleavage site of *VIPP1*-gRNA or *IFT46*-gRNA was added to both sides of the linker sequence and *YFP* coding sequence by using specific forward and reverse primers containing 25-bp micro-homologous arms (Table S3), respectively. The PCR product was purified using Gel Extraction Kit (QIAGEN) and concentrated with ethanol precipitation. The purified donor DNA was further quantified by NanoDrop 1000 spectrophotometer and adjusted concentration to ~500 ng μl^{-1}.

To prepare 96- or 98-bp short dsDNA donor with the 20-bp micro-homologous arms to the flank sequence of Cas9 cleavage site on *CrKU80*-gRNA1/-gRNA2/-gRNA3/-gRNA4, *CrTET1*-gRNA, *CrTET4*-gRNA, *VIPP1*-gRNA, *IFT46*-gRNA, *FTSY*-gRNA, *MAA7*-UTR-gRNA and *VIPP1*-UTR-gRNA loci, the ordered 96- or 98-nt sense and antisense oligonucleotides including the micro-homologous arm and a 56-nt DNA sequence containing three stop codons or a 51-nt DNA sequence encoding FLAG-HA epitope tag were annealed by incubating in the boiling water for 10 min, followed by cooling to room temperature. A total of 50 pmol of annealed short dsDNA donors were used per transformation. To prepare 346-bp, 438-bp and 360-bp dsDNA donors contained short homologous arms to the flank sequence of the Cas9 cleavage site on *FLA3*, *FLA10* and *FTSY* loci, the bridge-PCR was performed using the left and right homologous arms as templates. The substituted base is included in the 154-bp (FLA3) or 200-bp (FLA10) left homologous arm or 161-bp (FTSY) right homologous arm, resulting in the amino acid substitution Phe753Leu or Asn329Lys or Glu290stop codon. The exogenous 38-bp sequence (Table S3) was located in the middle of the donor. The PCR product was purified with Gel Extraction Kit (QIAGEN), concentrated with ethanol precipitation, and adjusted concentration to ~200 ng μl^{-1}.

Transformation of *Chlamydomonas reinhardtii* cells

Chlamydomonas reinhardtii 5×10^6 cells were washed twice in 1 ml Max Efficiency Transformation Reagent (Thermo Scientific) and suspended in 80 μl same reagent supplemented with 60 mM sorbitol. Purified SpCas9 (50 μg, 0.53 nmol) in storage buffer (20 mM HEPES, pH 7.5, 150 mM KCl, 1 mM DTT and 10% glycerol) was pre-incubated with gRNA (1.6 nmol) at a 1:3 molar ratio at 37°C for 15 min to form RNP complexes. For transformation of *C. reinhardtii*, 80 μl cell cultures (5×10^6 cells) together with 20 μl pre-incubated RNPs were mixed either with 12 pmol short or 2 μg (~7.5–9 pmol) modified or 4 μg (~8 pmol) YFP dsDNA donor and 2 μg (~1.7 pmol) Hm^R or Pm^R expression cassette. The molar ratio between the above multiple types of DNA donors and long selection marker DNA was about 4.5:1 (7.5/1.7) to 7:1 (12/1.7) (Table S1). Cells were electroporated in 4-mm cuvettes (600 V, 50 μF and resistance 300–400 ohm) using BTX Gemini System (HARVARD APPARATUS, Boston, MA, USA). Immediately after electroporation, 500 μl of TAP medium with 60 mM sorbitol was added. Cells were recovered overnight in 10 ml TAP with 60 mM sorbitol shaking at 120 rpm under continuous low light and then plated onto TAP-agar solid media supplemented with 10 μg ml^{-1} hygromycin or paromomycin and grown under 50 μmol photons m^{-2} sec^{-1} constant illumination. The Hm^R/or Pm^R colonies appeared after 7–10 days. For co-targeting *MAA7* & *FKB12*, *MAA7* & *IFT46*, *MAA7* & *FTSY* and *MAA7* & *CrKU80* in CC-5325 strain, 5×10^6 cells were mixed with each RNP together before electroporation. TAP-agar solid medium containing 20 μM 5-FI (Sigma, Saint Louis, MO, USA) was used to select the transformants resistant to 5-FI.

Determination of donor DNA integration at the cell population level using nested PCR

After 24 h of recovery, a fifth of the electroporated cells was harvested by centrifugation for 3 min at 1146 *g*. The cell pellet was prepared as a crude genomic lysate using the TransDirect Plant Tissue PCR Kit (TransGen Biotech). For the first round of nested PCR amplification, 4 μl crude genomic lysate was used as a template in a 50 μl volume of PCR reaction using Gflex high-fidelity DNA polymerase (Takara). The conditions for PCR amplification were as follows: an initial denaturation (95°C, 5 min); 20 cycles of denaturation (95°C, 30 sec), annealing (56°C, 30 sec) and elongation (68°C, 25 sec); final elongation (68°C, 7 min). Subsequently,

the 2 μl PCR product of the first-round amplification was used as a template for the second-round PCR amplification under the following conditions: an initial denaturation (95°C, 5 min); 35 cycles of denaturation (95°C, 30 sec), annealing (60°C, 30 sec) and elongation (68°C, 20 sec); final elongation (68°C, 7 min). The size of the PCR product was determined using 2% agarose gel. If necessary, the PCR products of second-round PCR were purified through the QIAquick PCR purification Kit (QIAGEN) and sequenced.

To determine whether donor DNA integration at colonies pools by nested PCR, all resistant colonies were divided into nine pools, and colonies from each pool were re-inoculated into a new TAP-agar plate. After 2 days of growth, a small number of cells from each colony was selected with a sterilized toothpick and suspended in 2 ml TAP medium. After 24 h of continuous culture, all cells were harvested and prepared as crude genomic DNA extracts. Nested PCR was then performed according to the method described above. Subsequently, the nested PCR products were analyzed using agarose gel and identified the pool in which the right size of PCR products was amplified for further analysis.

Genotypic analysis of resistant colonies

To determine whether the integration occurs in each resistant colony, the appropriate number of cells were selected from each colony, and the crude genomic DNA was prepared according to the method described above. Using crude genomic DNA as a template, colony PCR was performed using the inner primers of nested PCR for each target gene. After the agarose gel analysis of the obtained PCR products, the colonies with the expected size of PCR products were picked. Subsequently, the crude genomic DNA from selected colonies were used as templates to amplify the full-length donor DNA using gene-specific primers. The PCR products were then analyzed using 1% or 2% agarose gel to further confirm the complete donor DNA was integrated into the Cas9 cleavage site. Meanwhile, all the PCR products were purified and used for DNA sequencing.

Analysis of the gene's mRNA expression by reverse transcription-quantitative PCR (RT-qPCR)

According to the instruction manual, total RNA from *C. reinhardtii* was extracted using TrizolTM (Thermo, Waltham, MA, USA), and 1 μg RNA was used for subsequent cDNA synthesis using random hexamer & oligo dT primer mixes in the PrimeScriptTM RT reagent Kit with gDNA Eraser (TaKaRa). To analyze the expression of each target gene quantitatively, qRT-PCR was performed using 50 ng cDNA, NovoStart SYBR qPCR SuperMix (Novoprotein, Shanghai, China) and gene-specific primers (Table S3) for 40 cycles with CFX96TM Real-Time System (BIO-RAD). A gene encoding *Chlamydomonas* beta subunit-like polypeptide (*CBLP*) was used as the endogenous control. Data were analyzed with Bio-Rad CFX Manager (BIO-RAD), and expression levels relative to *CBLP* were determined with the formula $2^{-\Delta Ct}$.

Genomic DNA extraction

Total DNA was isolated using the CTAB method described by Sambrook et al. (1982). Briefly, cells were harvested, resuspended in a microprep buffer containing 2.5 × extract buffer (0.35 M Sorbitol, 0.1 M Tris–HCl pH 7.5 and 5 mM EDTA), 2.5 × nuclei lysis buffer [0.2 M Tris–HCl pH 7.5, 0.05 M EDTA, 2 M NaCl and 2% (w/v) CTAB] and 1 × 5% N-lauroylsarcosine, and incubated for 2 h at 65°C. The genomic DNA was extracted with chloroform:isoamyl alcohol (24:1) and precipitated with isopropanol. The DNA pellet was dissolved in nuclease-free water for further analysis.

Flagellar length measurements and microscopy

The methods of flagellar length measurements for *FLA3* F753L and *FLA10* N329K strains were described previously (Wang et al., 2019). For morphological observation and flagellar length measurement, the cells of *MAA7* and *MAA7IFT46* double mutants, and *FLA3* F753L and *FLA10* N329K strains were fixed and stained for 10 min at room temperature using 1% Lugol's solution (Shanghai Yuan Mu Biotechnology, Shanghai, China). The stained cells were then spread out on a slide and photographed using Olympus BX51 microscopic imaging system (Olympus, Tokyo, Japan).

Western blot analysis

The proteins in whole cells were extracted as described previously (Fowkes & Mitchell, 1998; Hu et al., 2014). After centrifugation, the proteins in supernatants were quantified and loaded onto a 10% SDS–PAGE gel. Then the proteins were blotted onto a nitrocellulose membrane. Membranes were blocked for 0.5 h with 5% milk in TBST and then incubated with anti-VIPP1 polyclonal antibody (Hu et al., 2014) or anti-IFT46 polyclonal antibody (Lv et al., 2017) or anti-FLAG monoclonal antibody (Sigma) or anti-HA monoclonal antibody (Cell Signaling Technology, Boston, MA, USA), anti-GFP monoclonal antibody (Roche, Basel, Switzerland) or anti-α-tubulin monoclonal antibody (Sigma) for 1 h and then rinsed three times for 5 min before incubation with peroxidase-conjugated goat anti-rabbit IgG (Jackson, Bar Harbor, ME, USA) or peroxidase-conjugated goat anti-mouse IgG (Jackson) for 1 h. The blots were developed with an ECL detection reagent (Millipore), and images of the blots were obtained using a CCD imager (Thermo).

Immunofluorescence staining

Immunofluorescence staining of *Chlamydomonas* cells was performed as detailed previously (Engel et al., 2012). Images of immune-stained samples were captured on a Leica TCS SP8 confocal microscope equipped with a 63 × oil-immersion lens. The excitation/emission parameters were as follows: DAPI, 405/423–488 nm; FITC, 488/495–545 nm; Alexa-Fluor-594, 552/612–671 nm. Brightness and contrast were adjusted using Carl Zeiss Zen 2009 Light Edition, Leica LAS AF 2.6.3 software.

Live-cell imaging of *IFT46-YFP* and *VIPP1-YFP* strains

Subcellular localization of the IFT46-YFP and VIPP1-YFP fusion proteins was visualized by laser-scanning confocal microscopy (Leica TCS SP8, Leica Microsystems, Wetzlar, Germany). YFP fluorescence was measured by the TauGating method (gating time = 0.5–10 nsec) to remove chlorophyll autofluorescence. The images were processed with Lightning software. Emission spectra for chloroplast autofluorescence and YFP were measured at 514 nm. Excitation spectra for chloroplast autofluorescence and YFP were measured at 650–700 nm and 520–570 nm, respectively.

ACCESSION NUMBERS

The accession numbers for all *Chlamydomonas* target genes used in this study were provided: *CrTET1*, *Cre12.g553400*; *CrKU80*, *Cre10.g423800*; *FKB12*, *Cre13.g586300*, *VIPP1*, *Cre13.g583550*; *IFT46*, *Cre05.g241637*; *FLA3*, *Cre10.g449250*; *FLA10*, *Cre17.g730950*; *FTSY*, *Cre05.g241450*; and *MAA7*, *Cre03.g161400*.

AUTHOR CONTRIBUTIONS

G-LX, K-YH and HC conceived the project. HC designed the study and developed microhomology-mediated donor DNA integration strategies, and performed most of the experiments and analyses. Q-LY and J-XX established the recombinant Cas9 purification protocols. X-JZ and TL selected and characterized the resistant colonies. Q-LY performed the Western blot analysis. XD performed immunofluorescence staining and live-cell imaging. MGR provided important suggestions for this study. HC wrote the manuscript, with input from G-LX and K-YH. All authors read and approved the final manuscript.

ACKNOWLEDGEMENTS

The authors would like to thank Dr Jia Chen for providing the pET28a-SpCas9 expression plasmid, and Dr Bei Yang for her assistance in the purification of Cas9. The authors thank Dr Yanhui Xu for providing the pPEI-His-Sumo vector. The authors thank Xiaojie Zhang and Ziyang Jin for participating in the identification of the genotype of the partial Hm^R colonies. The authors thank Fang Zhou from the Institute of Hydrobiology, C.A.S. for helping with microscopy experiments. The authors also thank Dr Fei Li for the project discussions. The authors are especially grateful to Prof. Donald Weeks and Prof. Graham Peers for their critical reading, revision and comments on this manuscript. This work was supported by the National Key R&D Program of China (2018YFA0800302 to G.X.), the National Science Foundation of China (31830018 to G.X.), Chinese Academy of Sciences (XDB19010102 to G.X.), National Nature Science Foundation of China (Grant 31871358 to Huang K), the Chinese National Key Research and Development Project for Synthetic Biology (2018YFA0902500), and Heye Health Technology Inc.

CONFLICT OF INTEREST

All authors declare no conflict of interest.

SUPPORTING INFORMATION

Additional Supporting Information may be found in the online version of this article.

Figure S1. The co-selection strategy with *MAA7* was used to obtain the mutants for the genes with different expression levels.

Figure S2. Co-selection with a drug resistance marker increased the ratio of mutants with donor DNA integration in two low-expression target genes.

Figure S3. Putative mutants with donor DNA integrated into the *CrKU80*, *VIPP1*, *IFT46*, *FLA3*, *FLA10* and *FTSY* genes were isolated from randomly selected Hm^R colonies.

Figure S4. Micro-homologous arm mediated precise knock-in of DNA donor containing stop codons in *FTSY* gene in the CC-1328 strain.

Figure S5. High-resolution images of plates #1 and #2 were used to count the number of all obtained Hm^R colonies from wild-type cells co-electroporeted with the *FTSY*-gRNA/Cas9 RNP, dsDNA donor and a Hm^R gene expression cassette.

Figure S6. Knock-in a *FLAG-HA* epitope tag in the low-expression genes *CrKU80* and *CrTET1*.

Figure S7. Insertion of a 38-bp DNA fragment into an intron did not affect mRNA maturation and the gene expression of *FLA3* and *FLA10*.

Figure S8. The average flagella length of CC-5325, *FLA3* F753L and *FLA10* N329K cells at 21°C and 33°C.

Figure S9. Short homologous arm mediated precise substitution of amino acids for FTSY in the CC-1328 strain.

Figure S10. Micro-homologous donor-mediated deletion of DNA fragments from the 3′-UTR of *MAA7*.

Figure S11. Micro-homologous donor-mediated precise deletion of a genomic region encoding the 3′-UTR of *MAA7*.

Figure S12. Micro-homologous donor-mediated precise deletion of a genomic region encoding the 3′-UTR of *VIPP1*.

Figure S13. Overview of the methods for multiple types of precise gene editing in *Chlamydomonas*.

Table S1. Summary of the combination of short dsDNA donor (Repair template) and long dsDNA (Selection marker) for each figure in this study

Table S2. Comparison of total editing efficiency of the method presented in this study with published methods

Table S3. List of the primers and DNA fragments used in this study

Table S4. DNA sequence of #5 and #33 *CrTET1* mutants

REFERENCES

Akella, S., **Ma, X.**, **Bacova, R.**, **Harmer, Z.P.**, **Kolackova, M.**, **Wen, X.** ***et al.*** (2021) Co-targeting strategy for precise, scarless gene editing with CRISPR/Cas9 and donor ssODNs in *Chlamydomonas*. *Plant Physiology*, **187**, 2637–2655.

Angstenberger, M., **de Signori, F.**, **Vecchi, V.**, **Dall'Osto, L.** & **Bassi, R.** (2020) Cell synchronization enhances nuclear transformation and genome editing via Cas9 enabling homologous recombination in *Chlamydomonas reinhardtii*. *ACS Synthetic Biology*, **9**, 2840–2850.

Bae, S., **Kweon, J.**, **Kim, H.S.** & **Kim, J.S.** (2014) Microhomology-based choice of Cas9 nuclease target sites. *Nature Medicine*, **11**, 705–706.

Baek, K., **Kim, D.H.**, **Jeong, J.**, **Sim, S.J.**, **Melis, A.**, **Kim, J.S.** ***et al.*** (2016) DNA-free two-gene knock-out in *Chlamydomonas reinhardtii* via CRISPR-Cas9 ribonucleoproteins. *Scientific Reports*, **6**, 30620.

Cheng, X., **Liu, G.**, **Ke, W.**, **Zhao, L.**, **Lv, B.**, **Ma, X.** ***et al.*** (2017) Building a multipurpose insertional mutant library for forward and reverse genetics in *Chlamydomonas*. *Plant Methods*, **13**, 36.

Chereji, R.V., **Kan, T.W.**, **Grudniewska, M.K.**, **Romashchenko, A.V.**, **Berezikov, E.**, **Zhimulev, I.F.** ***et al.*** (2016) Genome-wide profiling of nucleosome sensitivity and chromatin accessibility in Drosophila melanogaster. *Nucleic Acids Research*, **44**, 1036–1051.

Chudakov, D.M., **Lukyanov, S.** & **Lukyanov, K.A.** (2005) Fluorescent proteins as a toolkit for in vivo imaging. *Trends in Biotechnology*, **23**, 605–613.

Dhokane, D., **Bhadra, B.** & **Dasgupta, S.** (2020) CRISPR based targeted genome editing of *Chlamydomonas reinhardtii* using programmed Cas9-gRNA ribonucleoprotein. *Molecular Biology Reports*, **47**, 8747–8755.

Engel, B.D., **Ishikawa, H.**, **Wemmer, K.A.**, **Geimer, S.**, **Wakabayashi, K.-I.**, **Hirono, M.** ***et al.*** (2012) The role of retrograde intraflagellar transport in flagellar assembly, maintenance, and function. *The Journal of Cell Biology*, **199**, 151–167.

Ferenczi, A., **Chew, Y.P.**, **Kroll, E.**, **Koppenfels, C.**, **Hudson, A.** & **Molnar, A.** (2021) Mechanistic and genetic basis of single-strand templated repair at Cas12a-induced DNA breaks in Chlamydomonas reinhardtii. *Nature Communications*, **12**, 6751.

Ferenczi, A., **Pyott, D.E.**, **Xipnitou, A.** & **Molnar, A.** (2017) Efficient targeted DNA editing and replacement in *Chlamydomonas reinhardtii* using Cpf1 ribonucleoproteins and single-stranded DNA. *Proceedings of the National Academy of Sciences of the United States of America*, **114**, 13567–13572.

Findinier, J., **Delevoye, C.** & **Cohen, M.M.** (2019) The dynamin-like protein Fzl promotes thylakoid fusion and resistance to light stress in *Chlamydomonas reinhardtii*. *PLoS Genetics*, **15**, e1008047.

Fowkes, M.E. & **Mitchell, D.R.** (1998) The role of preassembled cytoplasmic complexes in assembly of flagellar dynein subunits. *Molecular Biology of the Cell*, **9**, 2337–2347.

Gorman, D.S. & **Levine, R.P.** (1965) Cytochrome f and plastocyanin: their sequence in the photosynthetic electron transport chain of *Chlamydomonas reinhardtii*. *Proceedings of the National Academy of Sciences of the United States of America*, **54**, 1665–1669.

Greiner, A., **Kelterborn, S.**, **Evers, H.**, **Kreimer, G.**, **Sizova, I.** & **Hegemann, P.** (2017) Targeting of photoreceptor genes in *Chlamydomonas reinhardtii* via Zincfinger nucleases and CRISPR/Cas9. *The Plant Cell*, **29**, 2498–2518.

Guzmán-Zapata, D., **Sandoval-Vargas, J.M.**, **Macedo-Osorio, K.S.**, **Salgado-Manjarrez, E.**, **Castrejón-Flores, J.L.**, **Oliver-Salvador, M.D.C.** ***et al.*** (2019) Efficient editing of the nuclear APT reporter gene in *Chlamydomonas reinhardtii* via expression of a CRISPR-Cas9 module. *International Journal of Molecular Sciences*, **20**, 1247.

Hayashi, A. & **Tanaks, K.** (2019) Short-homology-mediated CRISPR/Cas9 based method for genome editing in fission yeast. *G3: Genes, Genomes, Genetics*, **9**, 1153–1163.

Hisano, Y., **Sakuma, T.**, **Nakade, S.**, **Ohqa, R.**, **Ota, S.**, **Okamoto, H.** ***et al.*** (2015) Precise in-frame integration of exogenous DNA mediated by CRISPR/Cas9 system in zebrafish. *Scientific Reports*, **5**, 8841.

Hockemeyer, D., **Wang, H.**, **Kiani, S.**, **Lai, C.S.**, **Gao, Q.**, **Cassady, J.P.** ***et al.*** (2011) Genetic engineering of human pluripotent cells using TALE nucleases. *Nature Biotechnology*, **29**, 731–734.

Hou, Y., **Qin, H.**, **Follit, J.A.**, **Pazour, G.J.**, **Rosenbaum, J.L.** & **Witman, G.B.** (2007) Functional analysis of an individual IFT protein: IFT46 is required for transport of outer dynein arms into flagella. *The Journal of Cell Biology.*, **5**, 653–665.

Hu, J., **Deng, X.**, **Shao, N.**, **Wang, G.** & **Huang, K.** (2014) Rapid construction and screening of artificial microRNA systems in *Chlamydomonas reinhardtii*. *The Plant Journal*, **79**, 1052–1064.

Jakočiūnas, T., **Bonde, I.**, **Herrgård, M.**, **Harrison, S.J.**, **Kristensen, M.**, **Pedersen, L.E.** ***et al.*** (2015) Multiplex metabolic pathway engineering using CRISPR/Cas9 in *saccharomyces cerevisiae*. *Metabolic Engineering*, **28**, 213–222.

Jensen, T.K., **Fløe, L.**, **Petersen, S.T.**, **Huang, J.**, **Xu, F.**, **Bolund, L.** ***et al.*** (2017) Chromatin accessibility and guide sequence secondary structure affect CRISPR-Cas9 gene editing efficiency. *FEBS Letters*, **591**, 1892–1901.

Jeong, J., **Baek, K.**, **Yu, J.**, **Kirst, H.**, **Betterle, N.**, **Shin, W.** ***et al.*** (2018) Deletion of the chloroplast LTD protein impedes LHCI import and PSI-LHCI assembly in *Chlamydomonas reinhardtii*. *Journal of Experimental Botany*, **69**, 1147–1158.

Jiang, C. & **Pugh, B.F.** (2009) Nucleosome positioning and gene regulation: advances through genomics. *Nature Reviews. Genetics*, **10**, 161–172.

Jiang, W., **Brueqqeman, A.J.**, **Horken, K.M.**, **Plucinak, T.M.** & **Weeks, D.P.** (2014) Successful transient expression of Cas9 and single guide RNA genes in *Chlamydomonas reinhardtii*. *Eukaryotic Cell*, **13**, 1465–1469.

Jiang, W., **Zhou, H.**, **Bi, H.**, **Fromm, M.**, **Yang, B.** & **Weeks, D.P.** (2013) Demonstration of CRISPR/Cas9/sgRNA-mediated targeted gene modification in Arabidopsis, tobacco, sorghum and rice. *Nucleic Acids Research*, **41**, e188.

Jiang, W.Z. & **Weeks, D.P.** (2017) A gene-within-a-gene Cas9/sgRNA hybrid construct enables gene editing and gene replacement strategies in *Chlamydomonas reinhardtii*. *Algal Research*, **26**, 474–480. Available from: https://doi.org/10.1016/j.algal.2017.04.001

Kim, J., **Lee, S.**, **Baek, K.** & **Jin, E.** (2020) Site-specific gene knock-out and on-site heterologous gene overexpression in *Chlamydomonas reinhardtii* via a CRISPR-Cas9-mediated knock-in method. *Frontiers in Plant Science*, **11**, 306.

Li, C., **Chen, C.**, **Chen, H.**, **Wang, S.**, **Chen, X.** & **Cui, Y.** (2018) Verification of DNA motifs in Arabidopsis using CRISPR/Cas9-mediated mutagenesis. *Plant Biotechnology Journal*, **16**, 1446–1451.

Li, Y., **Fu, X.**, **Liu, D.** & **Liang, C.** (2004) Opening the chromatin for transcription. *The International Journal of Biochemistry & Cell Biology*, **36**, 1411–1423.

Liu, Z., **Hui, Y.**, **Shi, L.**, **Chen, Z.**, **Xu, X.**, **Chi, L.** ***et al.*** (2016) Efficient CRISPR/Cas9-mediated versatile, predictable, and donor-free gene knockout in human pluripotent stem cells. *Stem Cell Reports*, **7**, 496–507.

Lv, B., **Wan, L.**, **Taschner, M.**, **Cheng, X.**, **Lorentzen, E.** & **Huang, K.** (2017) Intraflagellar transport protein IFT52 recruits IFT46 to the basal body and flagella. *Journal of Cell Science*, **130**, 1662–1674.

Mali, P., **Yang, L.**, **Esvelt, K.M.**, **Aach, J.**, **Guell, M.**, **DiCarlo, J.E.** ***et al.*** (2013) RNA-guided human genome engineering via Cas9. *Science*, **339**, 823–826.

McVey, M. & **Lee, S.E.** (2008) MMEJ repair of double-strand breaks (director's cut): deleted sequences and alternative endings. *Trends in Genetics*, **24**, 529–538.

Merchant, S.S., **Prochnik, S.E.**, **Vallon, O.**, **Harris, E.H.**, **Karpowicz, S.J.**, **Witman, G.B.** ***et al.*** (2007) The *Chlamydomonas* genome reveals the evolution of key animal and plant functions. *Science*, **318**, 245–250.

Molnár, A., **Bassett, A.**, **Thuenemann, E.**, **Schwach, F.**, **Karkare, S.**, **Ossowski, S.** ***et al.*** (2009) Highly specific gene silencing by artificial microRNAs in the unicellular alga Chlamydomonas reinhardtii. *The Plant Journal*, **58**, 165–174.

Mueller, J., **Perrone, C.A.**, **Bower, R.**, **Cole, D.G.** & **Porter, M.E.** (2004) The FLA3 KAP subunit is required for localization of Kinesin-2 to the site of flagellar assembly and Processive anterograde Intraflagellar transport. *Molecular Biology of the Cell*, **16**, 1341–1354.

Nakade, S., **Tsubota, T.**, **Sakane, Y.**, **Kume, S.**, **Sakamoto, N.**, **Obara, M.** ***et al.*** (2014) Microhomology-mediated end-joining-dependent integration of donor DNA in cells and animals using TALENs and CRISPR/Cas9. *Nature Communications*, **20**, 5560.

Neupert, J., **Gallaher, S.D.**, **Lu, Y.**, **Strenkert, D.**, **Segal, N.**, **Barahimipour, R.** ***et al.*** (2020) An epigenetic gene silencing pathway selectively acting on transgenic DNA in the green alga Chlamydomonas. *Nature Communications*, **11**, 6269.

Nordhues, A., **Schottler, M.A.**, **Unger, A.K.**, **Geimer, S.**, **Schonfelder, S.**, **Schmollinger, S.** ***et al.*** (2012) Evidence for a role of VIPP1 in the structural Organization of the Photosynthetic Apparatus in *Chlamydomonas*. *The Plant Cell*, **24**, 637–659.

Palombella, L.A. & **Dutcher, K.S.** (1998) Identification of the gene encoding the tryptophan synthase beta-subunit from *Chlamydomonas reinhardtii*. *Plant Physiology*, **117**, 455–464.

Picariello, T., **Hou, Y.**, **Kubo, T.**, **McNeill, N.A.**, **Yanagisawa, H.A.**, **Oda, T.** ***et al.*** (2020) TIM, a targeted insertional mutagenesis method utilizing CRISPR/Cas9 in *Chlamydomonas reinhardtii*. *PLoS One*, **15**, e0232594.

Ran, F.A., **Hsu, P.D.**, **Wright, J.**, **Agarwala, V.**, **Scott, D.A.** & **Zhang, F.** (2013) Genome engineering using the CRISPR-Cas9 system. *Nature Protocols*, **8**, 2281–2308.

Rohr, J., **Sarkar, N.**, **Balenger, S.**, **Jeong, B.R.** & **Cerutt, H.** (2004) Tandem inverted repeat system for selection of effective transgenic RNAi strains in *Chlamydomonas*. *The Plant Journal*, **40**, 611–621.

Sakuma, T., **Nakade, S.**, **Sakane, Y.**, **Suzuki, K.T.** & **Yamamoto, T.** (2016) MMEJ-assisted gene knock-in using TALENs and CRISPR-Cas9 with the PITCh systems. *Nature Protocols*, **11**, 118–133.

Sambrook, J., **Fritsch, F.E.** & **Maniatis, T.** (1982) *Molecular cloning: a laboratory manual*. New York: Cold Spring Harbor press.

Schmollinger, S., **Strenkert, D.** & **Schroda, M.** (2010) An inducible artificial microRNA system for Chlamydomonas reinhardtii confirms a key role for heat shock factor 1 in regulating thermotolerance. *Current Genetics*, **56**, 383–389.

Shamoto, N., **Narita, K.**, **Kubo, T.**, **Oda, T.** & **Takeda, S.** (2018) CFAP70 is a novel axoneme-binding protein that localizes at the outer dynein arm and regulates ciliary motility. *Cells*, **7**(9), 124.

Shin, S.E., **Lim, J.M.**, **Koh, H.G.**, **Kim, E.K.**, **Kang, N.K.**, **Jeon, S.** ***et al.*** (2016) CRISPR/Cas9-induced knockout and knock-in mutations in *Chlamydomonas reinhardtii*. *Scientific Reports*, **13**, 27810.

Singh, V., **Braddick, D.** & **Dhar, P.K.** (2017) Exploring the potential of genome editing CRISPR-Cas9 technology. *Gene*, **599**, 1–18.

Singh, V., **Gohil, N.**, **Ramírez García, R.**, **Braddick, D.** & **Fofié, C.K.** (2018) Recent advances in CRISPR-Cas9 genome editing technology for biological and biomedical investigations. *Journal of Cellular Biochemistry*, **119**, 81–94.

Sizova, I., **Kelterborn, S.**, **Verbenko, V.**, **Kateriya, S.** & **Hegemann, P.** (2021) Chlamydomonas POLQ is necessary for CRISPR/Cas9-mediated gene targeting. *G3 (Bethesda)*, **11**, jkab114.

Sodeinde, O.A. & **Kindle, K.L.** (1993) Homologous recombination in the nuclear genome of *Chamydomonas reinhardtii*. *Proceedings of the National Academy of Sciences of the United States of America*, **90**, 9199–9203.

Thompson, L.H. & **Schild, D.** (2001) Homologous recombinational repair of DNA ensures mammalian chromosome stability. *Mutation Research*, **477**, 131–153.

Vashishtha, M., **Walther, Z.** & **Hall, J.L.** (1996) The kinesin-homologous protein encoded by the *Chlamydomonas* FLA10 gene is associated with basal bodies and centrioles. *Journal of Cell Science*, **109**, 541–549.

Wang, Q.Y., **Zhao, P.**, **Long, H.**, **Deng, X.** & **Huang, K.Y.** (2019) Polyubiquitylation of α-tubulin at K304 is required for flagellar disassembly in *Chlamydomonas*. *Journal of Cell Science*, **132**, jcs229047.

Xue, J.H., **Chen, G.D.**, **Hao, F.**, **Chen, H.**, **Fang, Z.**, **Chen, F.F.** ***et al.*** (2019) A vitamin-C-derived DNA modification catalyzed by an algal TET homologue. *Nature*, **569**, 581–585.

Yang, H., **Wang, H.**, **Shivalila, C.S.**, **Cheng, A.W.**, **Shi, L.** & **Jaenisch, R.** (2013) One-step generation of mice carrying reporter and conditional alleles by CRISPR/Cas9-mediated genome engineering. *Cell*, **154**, 1370–1379.

Yao, X., **Wang, X.**, **Liu, J.**, **Hu, X.**, **Shi, L.**, **Shen, X.** ***et al.*** (2017) CRISPR/Cas9–mediated precise targeted integration In vivo using a double cut donor with short homology arms. *eBioMedicine*, **20**, 19–26.

Zhang, R., **Patena, W.**, **Armbruster, U.**, **Gang, S.S.**, **Blum, S.R.** & **Jonikas, M.C.** (2014) High-throughput genotyping of green algal mutants reveals random distribution of mutagenic insertion sites and endonucleolytic cleavage of transforming DNA. *The Plant Cell*, **26**, 1398–1409.

Zhao, T., **Wang, W.**, **Bai, X.** & **Qi, Y.** (2009) Gene silencing by artificial microRNAs in *Chlamydomonas*. *The Plant Journal*, **58**, 157–164.

Zhao, W., **Siegel, D.**, **Biton, A.**, **Tonqueze, O.L.**, **Zaitlen, N.**, **Ahituv, N.** ***et al.*** (2017) CRISPR-Cas9-mediated functional dissection of 3′-UTRs. *Nucleic Acids Research*, **45**, 10800–10810.

Zhao, W., **Steinfeld, J.B.**, **Liang, F.**, **Chen, X.**, **Maranon, D.G.**, **Jian Ma, C.** ***et al.*** (2017) BRCA1-BARD1 promotes RAD51-mediated homologous DNA pairing. *Nature*, **550**, 360–365.